Mott Physics in Correlated Lattices: A Dynamical Mean Field Theory Study

Author: Abdulrahman Anter
Supervisor: Dr. Marcello Civelli

Project Presented to the
M2: Quantum, Light, Matter, and Nanosciences Program
Condensed Matter and Its Interfaces Track
at Université Paris-Saclay

Conducted at Laboratoire de Physique des Solides (LPS), Orsay

December 27, 2025

Abstract

This thesis follows the Mott metal–insulator transition of the half-filled Hubbard model from every useful vantage point. In the weak-interaction limit we derive simple expressions that capture the familiar Fermi-liquid behaviour, while in the strong-interaction limit we show how the model reduces to an antiferromagnetic spin-exchange problem. These two analytical cornerstones pin down the physics at either end of the phase diagram.

To connect the two regimes we turn to dynamical mean-field theory, treating the lattice as an infinitely connected Bethe network whose simple density of states keeps the calculations transparent yet still mimics real three-dimensional oxides with many nearest neighbours. The numerical results trace, in a single framework, the loss of coherent quasiparticles, the appearance of Hubbard side-bands and the opening of the insulating gap. The predicted spectra and critical interaction strength line up well with the classic Mott system V_2O_3.

In combination, the analytic limits and the intermediate-coupling solution provide a coherent, start-to-finish narrative of how a weak-coupling Slater metal turns into a strong-coupling Mott insulator, and they deliver a set of benchmark results for future, more elaborate many-body calculations.

Acknowledgments

I would like to express my deepest gratitude to my supervisor, Dr. Marcello Civelli, for his invaluable guidance, support, and scientific insight throughout the project. His mentorship has shaped both my understanding and appreciation of theoretical condensed matter physics. I am thankful to the faculty and staff of the QLMN program at Université Paris-Saclay for creating an intellectually stimulating environment. Special thanks also go to my colleagues and friends at LPS for helpful discussions and support during this journey. Finally, I am indebted to my family for their continuous encouragement, patience, and belief in me.

À mes parents, avec gratitude

Contents

1 Introduction

In 1911, H. Kamerlingh Onnes discovered that the DC resistivity of a mercury wire abruptly drops to zero when cooled to a critical temperature $T_c \approx 4.2, \mathrm{K}$ [1]. This implies that if one induces a current in a superconducting ring, the current persists for an astronomically long time—far exceeding the age of the universe ($\sim 10^{10}$ years)—indicating that electrons flow without resistance. Two decades later, W. Meissner and R. Ochsenfeld discovered that superconductors exhibit perfect diamagnetism by completely expelling applied magnetic fields—an effect now known as the Meissner effect [2].

The standard theory that explains these so-called conventional superconductors is the BCS theory—a subject extensive enough to warrant its own monograph (see [3], [4])—though we can briefly outline its phenomenological basis here.

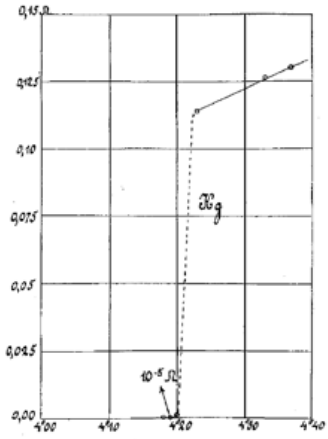

(a) DC resistivity of a mercury wire abruptly falls to zero at a critical temperature T_c of about 4.2K, from [1]

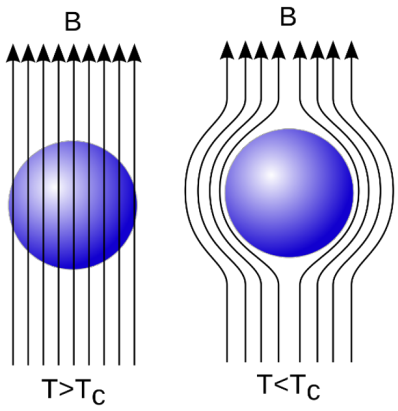

(b) Expulsion of magnetic flux (Meissner effect) in the superconducting state, from Wikipedia.

Figure 1: Experimental signatures of conventional superconductivity. Below the critical temperature, a material exhibits zero electrical resistance and expels magnetic fields from its interior (Meissner effect), demonstrating perfect diamagnetism.

Particles are classified as either bosons or fermions, depending on the symmetry of the system's wave function under the exchange of two identical particles: a symmetric wave function corresponds to bosons, while an antisymmetric one corresponds to fermions. This fundamental distinction is rooted in the quantum mechanical indeterminacy of particle trajectories [5]. As first anticipated by Pauli [6], particles with half-integer spin are classified as fermions, and those with integer spin as bosons.

Bosons can occupy the same single-particle quantum state, whereas fermions cannot—an outcome of the Pauli exclusion principle. This results in drastically different macroscopic behaviors: a system of non-interacting bosons can condense into the same ground state, giving rise to a new phase of matter known as the Bose–Einstein condensate (BEC). When weak interactions are introduced, such a condensate may exhibit superfluidity, a state of frictionless flow. The conceptual framework of superconductivity draws a close analogy to this behavior.

In our case, the system consists of fermions—specifically, conduction electrons—which do not condense in the usual sense. However, if pairs of electrons are formed, the resulting composite particles behave effectively as bosons and may undergo condensation. Yet, electrons repel each other via the Coulomb interaction; how can such pairing occur? The key lies in the underlying crystal lattice, which we have so far neglected. In 1950, E. Maxwell [7] and, independently, C. A. Reynolds et al. [8] observed that the critical temperature of superconductivity in mercury varies across its isotopes—elements that differ only in the number of neutrons, i.e., in lattice mass.

This pointed to the role of lattice vibrations. Fröhlich [9] and Bardeen [10] independently proposed that the lattice mediates an effective attractive interaction between electrons via phonons. Later, Cooper demonstrated that even an arbitrarily weak attractive interaction within a Fermi sea leads to a bound state of two electrons—what

we now call a Cooper pair [11]. These pairs act as bosonic degrees of freedom whose condensation underlies the phenomenon of superconductivity.

A few key points should be noted: the BCS theory describes weakly interacting electrons, which places an upper limit on the critical temperature, $T_c^{\max} \approx 30$K, for phonon-mediated superconductivity. In 1986, J. G. Bednorz and K. A. Müller [12] discovered a new superconducting material, $La_{2-x}Ba_xCuO_4$, a layered perovskite cuprate derived from La_2CuO_4 with partial substitution of La by Ba, exhibiting a critical temperature T_c of approximately 35K. Although this T_c only modestly exceeds the BCS limit, this was a surprise which casted strong doubt on the validity of BCS theory in these materials. The key point is that La_2CuO_4 is strongly correlated, meaning that electron–electron interactions dominate the physics. Moreover, the superconducting state in $La_{2-x}Ba_xCuO_4$ possesses an unconventional symmetry of the order parameter, classifying it as both a high-T_c and an unconventional superconductor.

This discovery marked the beginning of modern efforts to understand this new kind of superconductivity. The parent cuprate is already a rather unconventional state caractherized by the strong correlation and which is in an insulating phase, called Mott insulator, in sharp contrast with the prediction of the conventional band theory of solids. High-T_c superconductivity rises upon doping the Mott insulator. It is therefore generally believed that in order to understand high=T_C superconductivity first one has to understand the doping-driven metal– Mott insulator transition (MIT).

In this internship report, we begin by introducing the structure and phase diagram of cuprates, followed by a detailed review of the model of reference of these materials, the Hubbard model, and its analytical treatments. We then present a numerical investigation of the MIT using a more involved method, the Dynamical Mean-Field Theory (DMFT), which is able to well treat the strong correlation. We shall focus on its the phase diagram, and comparison to experimental observations.

2 Cuprates

$La_{2-x}Ba_xCuO_4$ belongs to a broader family of materials known as cuprates, which share a common layered crystal structure. These materials consist of CuO_2 planes separated by insulating spacer layers—often referred to as charge reservoirs in the context of doping (see Fig. 2a and reference [13]).

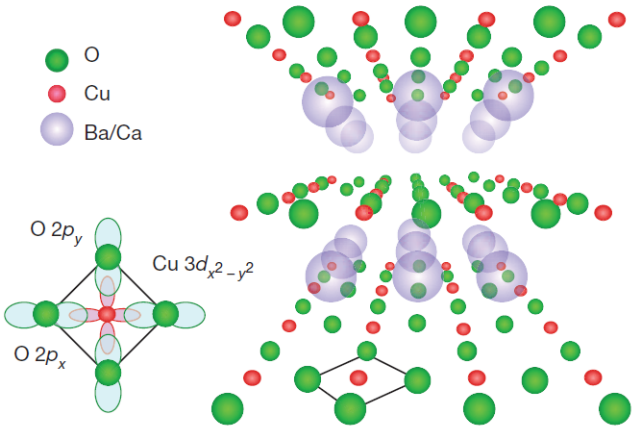

(a) Crystal structure: Layered copper oxides are composed of CuO_2 planes, typically separated by insulating spacer layers. The electronic structure of these planes primarily involves hybridization of a $3d_{x2-y2}$ hole on the copper sites with planar-coordinated $2p_x$ and $2p_y$ oxygen orbitals, from [13]

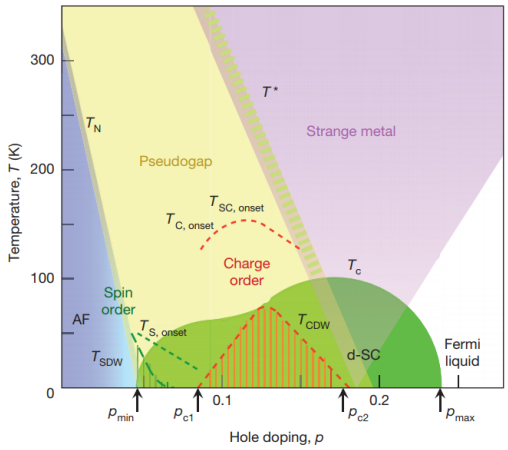

(b) Phase diagram: Temperature versus hole doping level for the copper oxides, indicating where various phases occur. The arrows indicate quantum critical points for superconductivity and charge order. From ref. [13]

Figure 2: Crystal structure $Ba_{2-x}Ca_xCuO_4$ and the phase diagram of Cuprates as a function of temperature and hole doping.

By varying the temperature T, the interaction strength U, or the doping level x, one can explore a rich and complex phase diagram (see Fig. 2b). A major focus of contemporary condensed matter physics is to understand the structure of such phase diagrams—specifically, the nature of the various phases, the (quantum) phase transitions between them, and the crossovers that connect different regimes.

In this work, we focus on a specific region of the canonical cuprate phase diagram: the parent state realized before hole-dopiong at $p = 0$, and study the correlation-driven metal–insulator transition.

3 The Hubbard Model

The Hubbard model is the standard theoretical framework for studying correlated electron behavior in cuprates. It is a tight-binding model in which electrons are primarily localized on atomic lattice sites and can move only via tunneling processes characterized by a hopping amplitude, typically denoted as $-t$. Electron–electron interactions are incorporated as an on-site Coulomb repulsion U, acting on a square lattice formed by the copper atoms, with a single active orbital per site. This defines the single-band Hubbard model, as expressed in Eq.(1) and illustrated in Fig.3.

The final term corresponds to the chemical potential, as we work in the grand canonical ensemble with a total of N lattice sites.

$$H = -t \sum_{\langle i,j\rangle\sigma} (c^\dagger_{j\sigma} c_{i\sigma} + c^\dagger_{i\sigma} c_{j\sigma}) + U \sum_j n_{j\uparrow} n_{j\downarrow} - \mu \sum_j (n_{j\uparrow} + n_{j\downarrow}) \tag{1}$$

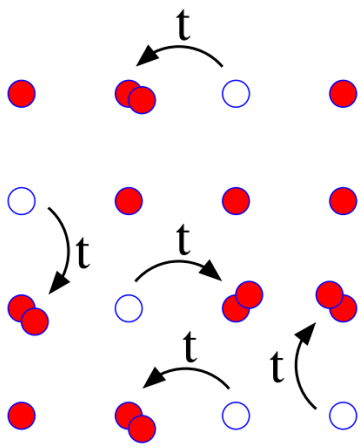

(a) Nearest-neighbor hopping between copper sites with a hopping amplitude $-t$.

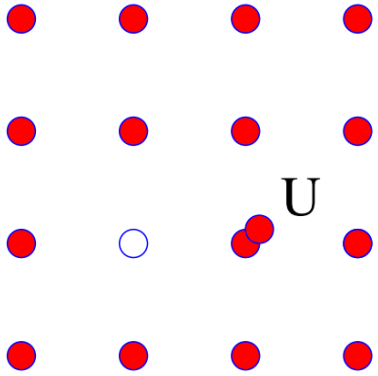

(b) Two electrons on the same site have an interaction energy U.

Figure 3: Pictorial representation of the first two terms in the Hubbard Hamiltonian, (1), from ref. [14]

The justification proceeds as follows: since the in-plane distances between atoms within the copper–oxide layers are much shorter than the distances between those planes and the oxygen atoms in the insulating layers (see Fig.4a), it is widely accepted that the essential physics occurs within the CuO_2 planes (see Fig.4b). The insulating spacer layers are typically regarded as charge reservoirs, supplying either electron or hole doping to the planes. Each copper atom hosts a $3d$ shell containing nine electrons, corresponding to ten nearly degenerate atomic states. In the crystal environment, this degeneracy is lifted by the surrounding lattice via crystal field effects. Consequently, the system is often approximated by retaining only a single active orbital per copper site. Finally, hopping between neighboring copper atoms is not direct, but rather mediated by the intermediate oxygen atoms. Nonetheless, it is conventional to describe this process as hopping between copper sites.

3.1 Particle–Hole Symmetry

Bipartite lattices, such as cubic and square lattices, have a special structure: they can be divided into two sublattices, $\mathcal{A}$ and $\mathcal{B}$, so that every site in one sublattice is connected only to sites in the other. In particular, each site in $\mathcal{A}$ is exclusively surrounded by sites in $\mathcal{B}$, and vice versa.

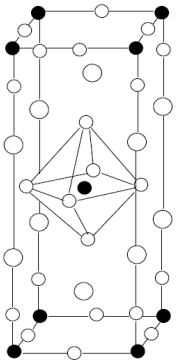

(a) This figure shows that the intra-copper oxides plane distances are much shorter than the distances between the planes and the oxygen atom in the insulating layers, from ref.[15]

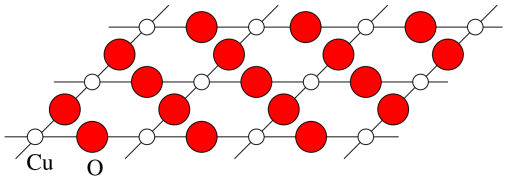

(b) Copper Oxide planes in cuprates, from ref. [16].

Figure 4

This bipartite structure naturally supports antiferromagnetic order, as it allows spin-up and spin-down electrons to preferentially occupy different sublattices without violating the Pauli exclusion principle.

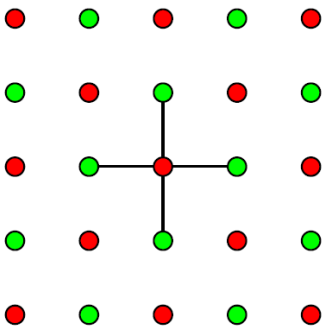

(a) The square lattice is a bipartite lattice which can be divided into two sublattices $\mathcal{A}$ (red) and $\mathcal{B}$ (green), from ref. [14]

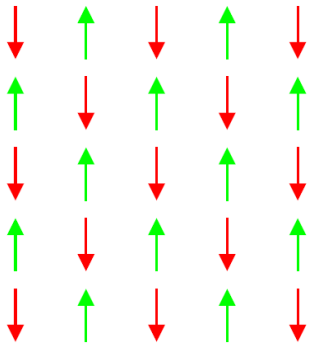

(b) The square lattice is a bipartite lattice and, naturally, it supports an antiferromagnetic order, since spin-up and spin-down electrons can occupy separate sublattices, from ref. [14]

Figure 5

We now introduce the particle–hole transformation (PHT):

$$c^\dagger_{j\sigma} \longrightarrow d^\dagger_{j\sigma} = (-1)^j c_{j\sigma} \tag{2}$$

$$c_{j\sigma} \longrightarrow d_{j\sigma} = (-1)^j c^\dagger_{j\sigma} \tag{3}$$

Here, the symbol "$\longrightarrow$" indicates that in the Hamiltonian, the operator on the left is to be replaced by the expression on the right. The factor $(-1)^j$ takes the value ± 1 depending on the sublattice to which site j belongs. For nearest neighbors i and j, which lie on opposite sublattices, we then have $(-1)^{i+j} = -1$.

Under this transformation, the following operator identities hold:

$$c^\dagger_{j\sigma}c_{i\sigma} \longrightarrow c^\dagger_{i\sigma}c_{j\sigma} \tag{4}$$

$$n_{j\sigma} = c^\dagger_{j\sigma}c_{j\sigma} \longrightarrow d^\dagger_{j\sigma}d_{j\sigma} = 1 - c^\dagger_{j\sigma}c_{j\sigma} = 1 - n_{j\sigma} \tag{5}$$

$$(c^\dagger_{j\sigma}c_{i\sigma} + c^\dagger_{i\sigma}c_{j\sigma}) \longrightarrow (c^\dagger_{i\sigma}c_{j\sigma} + c^\dagger_{j\sigma}c_{i\sigma}) \tag{6}$$

$$n_{j\uparrow}n_{j\downarrow} \longrightarrow 1 - n_{j\uparrow} - n_{j\downarrow} + n_{j\uparrow}n_{j\downarrow} \tag{7}$$

$$n_{j\uparrow} + n_{j\downarrow} \longrightarrow 2 - (n_{j\uparrow} + n_{j\downarrow}) \tag{8}$$

Putting these together, the terms in the Hubbard Hamiltonian transform as:

$$T = -t \sum_{\langle i,j\rangle\sigma} (c^\dagger_{j\sigma}c_{i\sigma} + c^\dagger_{i\sigma}c_{j\sigma}) \longrightarrow T' = T \tag{9}$$

$$V = U\sum_j (n_{j\uparrow} - \frac{1}{2})(n_{j\downarrow} - \frac{1}{2}) \longrightarrow V' = V - U\sum_j (n_{j\uparrow} + n_{j\downarrow}) + UN \tag{10}$$

$$-\mu\sum_j (n_{j\uparrow} + n_{j\downarrow}) \longrightarrow \mu\sum_j (n_{j\uparrow} + n_{j\downarrow}) - 2\mu N \tag{11}$$

$$H \longrightarrow H' = H - (U - 2\mu)\sum_j (n_{j\uparrow} + n_{j\downarrow}) + \sum_j (U - 2\mu) \tag{12}$$

The transformed Hamiltonian H' describes the dynamics of holes. It is clear that H is invariant under PHT only if $\mu = U/2$. Now consider the alternative but equivalent form of the Hubbard Hamiltonian:

$$H = -t \sum_{\langle i,j\rangle\sigma} (c^\dagger_{j\sigma}c_{i\sigma} + c^\dagger_{i\sigma}c_{j\sigma}) + U\sum_j (n_{j\uparrow} - \frac{1}{2})(n_{j\downarrow} - \frac{1}{2}) - \mu\sum_j (n_{j\uparrow} + n_{j\downarrow}) \tag{13}$$

This Hamiltonian differs from the standard form only by a shift in the chemical potential and an additive constant in the energy, as

$$U(n_{j\uparrow} - \frac{1}{2})(n_{j\downarrow} - \frac{1}{2}) = Un_{j\uparrow}n_{j\downarrow} - \frac{U}{2}(n_{j\uparrow} + n_{j\downarrow}) + \frac{U}{4} \tag{14}$$

Under PHT, both the kinetic and interaction terms in this form remain invariant. Only the chemical potential term changes sign (up to an additive constant):

$$-\mu\sum_j (n_{j\uparrow} + n_{j\downarrow}) \longrightarrow -2\mu N + \mu\sum_j (n_{j\uparrow} + n_{j\downarrow}) \tag{15}$$

Therefore, the Hamiltonian is PHT-invariant only at $\mu = 0$. The average site occupancy is defined as:

$$\rho = \frac{1}{N}\sum_j \langle n_{j\uparrow} + n_{j\downarrow}\rangle \tag{16}$$

Under PHT, this transforms as $\rho \to 2 - \rho$. Thus,

$$\rho(\mu) \longrightarrow \rho_h(\mu) = 2 - \rho(-\mu)_e \tag{17}$$

Since the system is symmetric under particle–hole transformation at $\mu = 0$, it follows that $\rho_e(0) = \rho_h(0)$. Hence,

$$\rho = 2 - \rho \Longrightarrow \rho = 1 \tag{18}$$

That is, $\mu = 0$ corresponds to half-filling.

3.2 Green's Functions

Green's functions are a class of correlation functions that play a central role in many-body theory and are particularly important for the analysis presented in this work. Suppose that the eigenstates of the full Hamiltonian H describing the system are labeled by λ. The Green's function (GF) is then defined as:

$$G(\lambda, t - t') = -i\,\langle Tc_\lambda(t)c^\dagger_\lambda(t')\rangle \tag{19}$$

Here, $c_\lambda(t)$ and $c_\lambda^\dagger(t')$ are annihilation and creation operators, respectively, for the H eigenstate λ. The operator T denotes time ordering—not temperature—and is defined such that, for example, for the generic operator $\hat{V}$:

$$T[\hat{V}(t_1)\hat{V}(t_2)\hat{V}(t_3)] = \hat{V}(t_3)\hat{V}(t_1)\hat{V}(t_2), \text{ if } t_3 > t_1 > t_2 \tag{20}$$

The expectation value is taken over the ground state at zero temperature or the canonical ensemble at finite temperatures. The definition is given in the Heisenberg picture, where operators evolve in time as:

$$c_\lambda(t) = e^{iHt} c_\lambda e^{-iHt} \tag{21}$$

A related quantity, particularly important for the description of experimental observables, is the spectral function, defined as

$$A_\lambda(\omega) = -2\Im G_\lambda^R(\omega) \tag{22}$$

$$A_\lambda(\omega) > 0 \tag{23}$$

$$1 = \int_{-\infty}^{\infty} \frac{d\omega}{2\pi} A_\lambda(\omega) \tag{24}$$

where $G_\lambda^R(\omega)$ is the Fourier transform of the retarded Green's function, given by:

$$G^R(\lambda, t-t') = -i\Theta(t-t') \left\langle \{c_\lambda(t), c_\lambda^\dagger(t')\}_\pm \right\rangle \tag{25}$$

Here, $\{\cdot,\cdot\}_\pm$ denotes the anticommutator (for fermions) or commutator (for bosons), and $\Theta(t-t')$ is the Heaviside step function. The spectral function $A_\lambda(\omega)$ can be interpreted as a resolved density of states, or more precisely, as a probability distribution that gives the likelihood of finding a particle in state λ with excitation energy ω.

In the following, we compute the Green's function and corresponding spectral function in two ways: first via the imaginary-time (Matsubara) formalism, and second using the spectral (Lehmann) representation. For further details, see, for example, ref. [4].

3.3 Single-Site Hubbard Model

To gain insight into the deceptively simple but analytically challenging Hubbard Hamiltonian eq. 13, we begin by considering a limiting case: $t = 0$, which corresponds to the absence of hopping between sites. This yields the so-called single-site Hubbard model:

$$H = U \sum_j (n_{j\uparrow} - \frac{1}{2})(n_{j\downarrow} - \frac{1}{2}) - \mu \sum_j (n_{j\uparrow} + n_{j\downarrow}) \tag{26}$$

In this limit, single-site number operators $n_{j\sigma}$ commute with the Hamiltonian; that is, $[H, n_{j\sigma}] = [n_{i\sigma}, n_{j\sigma}] = 0$. This implies that the Hamiltonian is separable, and we can analyze each site independently. The corresponding single-site Hamiltonian is:

$$H_{t=0} = U(n_{j\uparrow} - \frac{1}{2})(n_{j\downarrow} - \frac{1}{2}) - \mu(n_{j\uparrow} + n_{j\downarrow}) \tag{27}$$

This form of the Hamiltonian is equivalent to the atomic limit of the Anderson model (AIM), see chapter 16 in [17], which describes an isolated ion:

$$H = \underbrace{\sum_{\mathbf{k},\sigma} \epsilon_{\mathbf{k}} n_{\mathbf{k}\sigma} + \sum_{\mathbf{k},\sigma} \left[V(\mathbf{k}) c_{\mathbf{k}\sigma}^\dagger f_\sigma + V^*(\mathbf{k}) f_\sigma^\dagger c_{\mathbf{k}\sigma} \right]}_{H_{\text{resonance}}} + \underbrace{E_f n_f + U n_{f\uparrow} n_{f\downarrow}}_{H_{\text{atomic}}} \tag{28}$$

where $c_{\mathbf{k}\sigma}^\dagger$ and $f_\sigma^\dagger$ are creation operators for conduction and localized electrons, respectively, $V(\mathbf{k})$ is the hybridization amplitude, $\epsilon_{\mathbf{k}}$ the dispersion of conduction electrons, E_f the impurity level energy, and U the on-site Coulomb interaction. The AIM atomic limit is

$$H_{atomic} = E_f n_f + U n_{f\uparrow} n_{f\downarrow} \tag{29}$$

Noting that $H_{t=0}$ can be rewritten as:

$$H_{t=0} = Un_\uparrow n_\downarrow - (\frac{U}{2} + \mu)(n_\uparrow + n_\downarrow) + \frac{U}{4} \tag{30}$$

we see that the last term is a constant energy shift and can be ignored. The two Hamiltonians are therefore equivalent under the identification $E_f = U/2 + \mu$. For simplicity, we will proceed with H_{atomic}.

Since the model involves only a single site, the possible electronic configurations are:

$$|0,0\rangle, |1,0\rangle, |0,1\rangle, |1,1\rangle \tag{31}$$

where the first (second) entry in the ket denotes the number of spin-up (spin-down) electrons. The corresponding energies of these states are 0, E_f, E_f, and $2E_f + U$, respectively, with E_f being a two-fold degenerate level. The energy cost to add or remove an electron from this degenerate level is:

$$\Delta E_\pm = \frac{U}{2} \pm (E_f + \frac{U}{2}) \tag{32}$$

Provided that $\Delta E_\pm > 0$, or equivalently $U/2 > |E_f + U/2|$, the singly occupied states lie lower in energy than the empty or doubly occupied states. This implies that the ground state corresponds to a localized single electrons, which carry a magnetic moment. Returning to the single-site Hubbard Hamiltonian, we therefore expect localized moments on individual lattice sites with charge transport suppressed. We shall show that his is already the hallmark of a Mott insulator.

3.3.1 The Mott Insulator (An Insight)

To compute any thermodynamic quantity, we begin by evaluating the partition function Z, defined as:

$$Z = Tr[e^{-\beta H}] = \sum_\alpha \langle\alpha| e^{-\beta H} |\alpha\rangle \tag{33}$$

The energies of the four atomic states introduced earlier, expressed in terms of the Hubbard-Hamiltonian parameters, are:

$$E_{|0,0\rangle} = \frac{U}{4} \tag{34}$$

$$E_{|1,0\rangle} = E_{|0,1\rangle} = -\mu - \frac{U}{4} \tag{35}$$

$$E_{|1,1\rangle} = \frac{U}{4} - 2\mu \tag{36}$$

At $\mu = 0$, the energy levels simplify to:

$$E_{|0,0\rangle} = E_{|1,1\rangle} = \frac{U}{4} \tag{37}$$

$$E_{|1,0\rangle} = E_{|0,1\rangle} = -\frac{U}{4} \tag{38}$$

This reveals a particle–hole symmetric spectrum, consistent with our earlier discussion. The corresponding partition function becomes:

$$Z = e^{-\beta\frac{U}{4}} + e^{-\beta(\frac{U}{4} - 2\mu)} + 2e^{-\beta(-\frac{U}{4} - \mu)} \tag{39}$$

The average occupation of the site is given by the following:

$$\rho = \langle n_\uparrow + n_\downarrow \rangle = Z^{-1} Tr[(n_\uparrow + n_\downarrow) e^{-\beta H}] \tag{40}$$

$$= Z^{-1} Tr[2e^{\beta(\mu + \frac{U}{4})} + 2e^{-\beta(\frac{U}{4} - 2\mu)}] \tag{41}$$

At $\mu = 0$, the system is half-filled and we find $\rho = 1$. Figure 6 shows ρ as a function of μ for $U = 4$ and various temperatures. At sufficiently low temperatures, we observe a plateau centered around $\mu = 0$, where the occupation remains pinned at $\rho = 1$. This plateau corresponds to the Mott gap, and the system in this regime is referred to as a Mott insulator. Physically, this reflects the fact that adding or removing an electron requires an energy cost of the order U, needed to overcome the on-site interaction. As the temperature increases, thermal fluctuations begin to blur this gap, as seen in Fig. 6 for $T = 2K/k_B$.

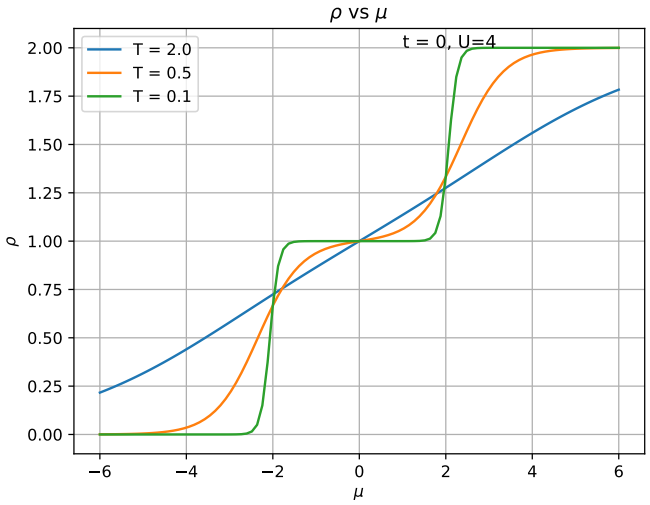

Figure 6: Plot of the average site occupancy, average density, in the single-site Hubbard model $t = 0$, for $U = 4$, showing an insulating behavior and the "Mott gap" near $\mu = 0$.

3.3.2 The Spectral Function

While calculating Green functions, it is often convenient to work on the complex plane, and in particular on the imaginary axis, especially when temperature is involved. Once the full Green's function has been determined, it is then possible to analytically continue it on the real axis, where observables are defined.

Imaginary-Time Approach The Matsubara (imaginary-time) Green's function is defined as:

$$G_\uparrow(\tau) = -\langle T_\tau c_\uparrow(\tau) c_\uparrow^\dagger(0)\rangle \tag{42}$$

where T_τ denotes the imaginary-time ordering operator, and the imaginary time τ lies within the interval $-\beta \leq \tau \leq \beta$. At $\mu = 0$, the Green's function becomes:

$$G_\uparrow(\tau) = -\Theta(\tau) Z^{-1}\left[e^{\beta\frac{U}{4}} e^{-\tau\frac{U}{2}} + e^{-\beta\frac{U}{4}} e^{\tau\frac{U}{2}}\right] + \Theta(-\tau) Z^{-1}\left[e^{-\beta\frac{U}{4}} e^{-\tau\frac{U}{2}} + e^{\beta\frac{U}{4}} e^{\tau\frac{U}{2}}\right]$$

We now take the Fourier transform using:

$$G_\uparrow(i\omega_n) = \int_0^\beta d\tau e^{i\omega_n\tau} G_\uparrow(\tau) \tag{43}$$

Substituting and evaluating the integral gives:

$$G_\uparrow(i\omega_n) = -Z^{-1}\left\{e^{\beta\frac{U}{4}} \int_0^\beta d\tau e^{i\omega_n\tau} e^{-\tau\frac{U}{2}} + e^{-\beta\frac{U}{4}} \int_0^\beta d\tau e^{i\omega_n\tau} e^{\tau\frac{U}{2}}\right\}$$

$$G_\uparrow(i\omega_n) = -Z^{-1}\left\{e^{\beta\frac{U}{4}} \frac{e^{(i\omega_n - \frac{U}{2})\beta} - 1}{i\omega_n - \frac{U}{2}} + e^{-\beta\frac{U}{4}} \frac{e^{(i\omega_n + \frac{U}{2})\beta} - 1}{i\omega_n + \frac{U}{2}}\right\}$$

For fermions, only odd Matsubara frequencies appear, and we use $e^{i\beta\omega_n} = -1$ to simplify:

$$G_\uparrow(i\omega_n) = Z^{-1}\left\{\frac{e^{\beta U/4} + e^{-\beta U/4}}{i\omega_n - \frac{U}{2}} + \frac{e^{\beta U/4} + e^{-\beta U/4}}{i\omega_n + \frac{U}{2}}\right\}$$

$$G_\uparrow(i\omega_n) = \frac{1}{2}\left\{\frac{1}{i\omega_n - \frac{U}{2}} + \frac{1}{i\omega_n + \frac{U}{2}}\right\} \tag{44}$$

We have thus obtained the Matsubara Green's function in the frequency domain. To compute the corresponding retarded Green's function, we perform analytic continuation via $i\omega_n \to \omega + i\eta$, where η is an infinitesimal positive quantity:

$$G_\uparrow^R(\omega) = \frac{1}{2}\left\{\frac{1}{\omega + i\eta - \frac{U}{2}} + \frac{1}{\omega + i\eta + \frac{U}{2}}\right\} \tag{45}$$

Using Cauchy's identity,

$$\lim_{\eta\to 0}\frac{1}{\omega-\epsilon\pm i\eta}=\mathcal{P}\big(\frac{1}{\omega-\epsilon}\big)\pm i\pi\delta(\omega-\epsilon) \tag{46}$$

we obtain the spectral function:

$$A(\omega)=\pi\big[\delta(\omega-\frac{U}{2})+\delta(\omega+\frac{U}{2})\big] \tag{47}$$

Lehmann Representation Approach The same result can be derived using the Lehmann representation [4], which expresses the retarded Green's function in terms of the eigenstates of the full interacting Hamiltonian:

$$G^R(\alpha,\omega)=Z^{-1}\sum_{n,m}|\langle n|c_\alpha|m\rangle|^2\frac{e^{-\beta E_n}+e^{-\beta E_m}}{\omega+i\eta+E_n-E_m} \tag{48}$$

where E_n and E_m are the energies of the states $|n\rangle$ and $|m\rangle$, respectively. Again, working at $\mu=0$ and considering only the states $|1,0\rangle$ and $|1,1\rangle$ that contribute, we obtain:

$$G^R_\uparrow(\omega)=Z^{-1}(e^{\beta U/4}+e^{-\beta U/4})\Big\{\frac{1}{\omega+i\eta-\frac{U}{2}}+\frac{1}{\omega+i\eta+\frac{U}{2}}\Big\} \tag{49}$$

which matches the earlier expression for $G^R(\omega)$ and yields the same spectral function $A(\omega)$ as in Eq.(18). This is shown in Fig.7 for $U=4$ and is consistent with the energy levels derived in Eq. (38). The two Dirac δ-functions represent the minimal excitation energies required to add or remove an electron from the singly-occupied ground state: $\pm U/2$, respectively. This confirms the earlier insight that charge transport requires overcoming a finite energy barrier—meaning the system is insulating.

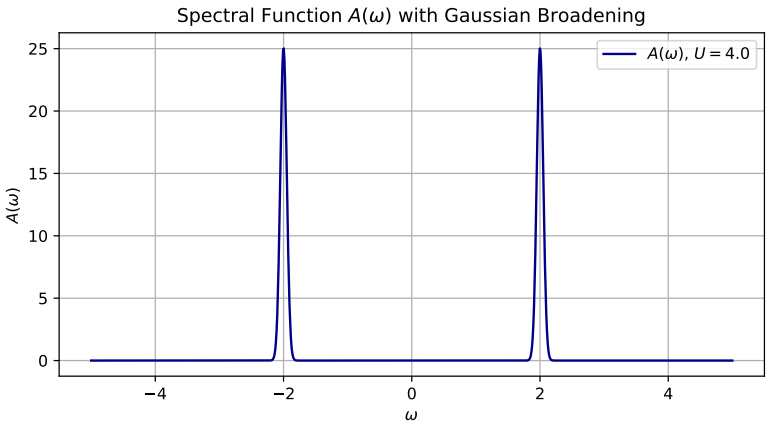

Figure 7: Plot of the single-site Hubbard Hamiltonian spectral function at $U=4$, showing that an electron or a hole excitation requires an energy $\pm U/2$, corresponding to the energy cost of adding or removing an electron at half-filling.

Finally, the spin-up occupation number on a single site can be computed via:

$$\begin{aligned}\langle n_\uparrow\rangle=\int_{-\infty}^{+\infty}\frac{d\omega}{2\pi}\frac{A(\omega)}{1+e^{-\beta\omega}}&=\int_{-\infty}^{+\infty}\frac{d\omega}{2}\frac{1}{1+e^{-\beta\omega}}\big[\delta(\omega-\frac{U}{2})+\delta(\omega+\frac{U}{2})\big]\\&=\frac{1}{2}\Big[\frac{1}{1+e^{-\beta\frac{U}{2}}}+\frac{1}{1+e^{\beta\frac{U}{2}}}\Big]\end{aligned} \tag{50}$$

As $T\to 0$ (or equivalently, $\beta\to\infty$), this expression approaches $1/2$, and by particle–hole symmetry, $\langle n_\downarrow\rangle=1/2$ as well. Hence, the total occupation becomes $\langle n_j\rangle=1$, consistent with the system residing in its lowest-energy configuration.

3.4 The Non-Interacting Hubbard Model: $U = 0$ Limit

It is instructive to study the physical properties of the Hubbard Model in the opposite limit of vanishing interaction strength ($U = 0$). In this case he Hubbard Hamiltonian reduces to a simple tight-binding form :

$$H_0 = -t \sum_{\langle i,j\rangle\sigma} (c^\dagger_{j\sigma} c_{i\sigma} + c^\dagger_{i\sigma} c_{j\sigma}) - \mu \sum_j (n_{j\uparrow} + n_{j\downarrow}) \tag{51}$$

The Hamiltonian is invariant under discrete lattice translations, implying that it commutes with momentum eigenstates. This allows us to diagonalize it using Fourier-transformed operators :

$$c^\dagger_{\mathbf{k},\sigma} = \frac{1}{\sqrt{N}} \sum_j e^{i\mathbf{k}.\mathbf{R_j}} c^\dagger_{j,\sigma} \tag{52}$$

$$c_{\mathbf{k},\sigma} = \frac{1}{\sqrt{N}} \sum_j e^{-i\mathbf{k}.\mathbf{R_j}} c_{j,\sigma} \tag{53}$$

$$c^\dagger_{j,\sigma} = \frac{1}{\sqrt{N}} \sum_{\mathbf{k}} e^{-i\mathbf{k}.\mathbf{R_j}} c^\dagger_{\mathbf{k},\sigma} \tag{54}$$

$$c_{j,\sigma} = \frac{1}{\sqrt{N}} \sum_{\mathbf{k}} e^{i\mathbf{k}.\mathbf{R_j}} c_{\mathbf{k},\sigma} \tag{55}$$

Using these relations, and noting that

$$\frac{1}{N} \sum_j e^{-i(\mathbf{k}-\mathbf{k}').\mathbf{R_j}} = \delta_{\mathbf{k}=\mathbf{k}'} \tag{56}$$

we obtain:

$$H_0 = \sum_{\mathbf{k},\sigma} \Big(-t \sum_{\delta\in(\pm\hat{x}a,\pm\hat{y}a)} e^{i\mathbf{k}.\delta} \Big) c^\dagger_{\mathbf{k},\sigma} c_{\mathbf{k},\sigma} - \mu \sum_{\mathbf{k}} n_{\mathbf{k}} \tag{57}$$

which can be expressed in the compact form:

$$H_0 = \sum_{\mathbf{k},\sigma} \xi_{\mathbf{k}} n_{\mathbf{k}} \tag{58}$$

$$\xi_{\mathbf{k}} = \epsilon_{\mathbf{k}} - \mu \tag{59}$$

$$\epsilon_{\mathbf{k}} = -2t\big\{cos(k_x a) + cos(k_y a)\big\} \tag{60}$$

where a is the lattice constant, and k_x, k_y are the components of the wavevector $\mathbf{k}$ along the $\hat{x}$ and $\hat{y}$ directions, respectively. The resulting dispersion relation gives rise to a divergent density of states at $\mu = 0$, which can be calculated via:

$$D(\epsilon) = \sum_{\mathbf{k}} \delta(\epsilon - \xi_{\mathbf{k}}) \tag{61}$$

The density of states is shown in Fig. 9. Throughout this work, the summation over wavevectors $\sum_{\mathbf{k}}$ is assumed to be normalized by the volume of the Brillouin zone. At half-filling ($\mu = 0$), with N electrons on N sites, the system occupies N states; we have a total of $2N$ states due to spin degeneracy. Based on this picture, one would expect the system to behave as a band conductor, as shown in Fig. 8a. ***However, this is not observed experimentally: undoped cuprates are good insulators. This indicates that electronic interactions cannot be neglected.*** The Fermi surface—defined by the condition $\xi_{\mathbf{k}} = 0$ or $\epsilon_{\mathbf{k}} = \mu$—is shown for various chemical potentials in Fig. 8b. Notably, at $\mu = 0$, the system exhibits perfect nesting at the wavevector $\mathbf{q} = (\pi, \pi)$. This means that large segments of the Fermi surface can be mapped onto each other under translation by $\mathbf{q}$. Such nesting enhances the susceptibility to antiferromagnetic (AFM) ordering in response to magnetic perturbations with wavevector $\mathbf{q}$, and motivates our subsequent mean-field treatment of magnetization density m.

3.4.1 The Spectral Function

The retarded Green's function for the non-interacting system is:

$$G^R(\mathbf{k}, \omega) = \frac{1}{\omega + i\eta - \xi_{\mathbf{k}}} \tag{62}$$

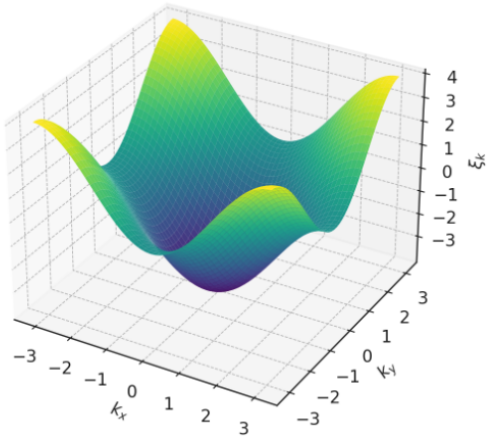

(a) Plot of the non-interacting Hubbard Hamiltonian dispersion in the 1^{st} BZ.

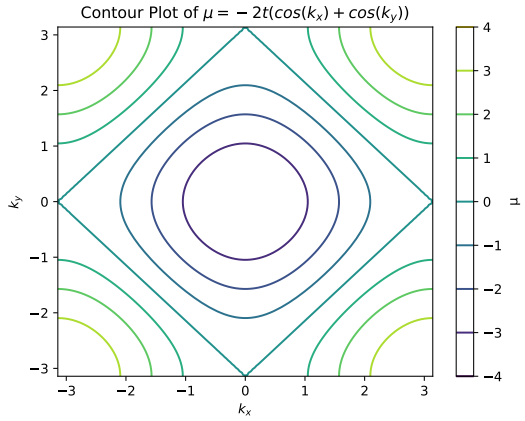

(b) Plot of different Fermi surfaces for the non-interacting Hubbard Hamiltonian for various values of μ: a square geometry at $\mu = 0$, and perfect nesting with a vector $\mathbf{q} = (\pi, \pi)$.

Figure 8

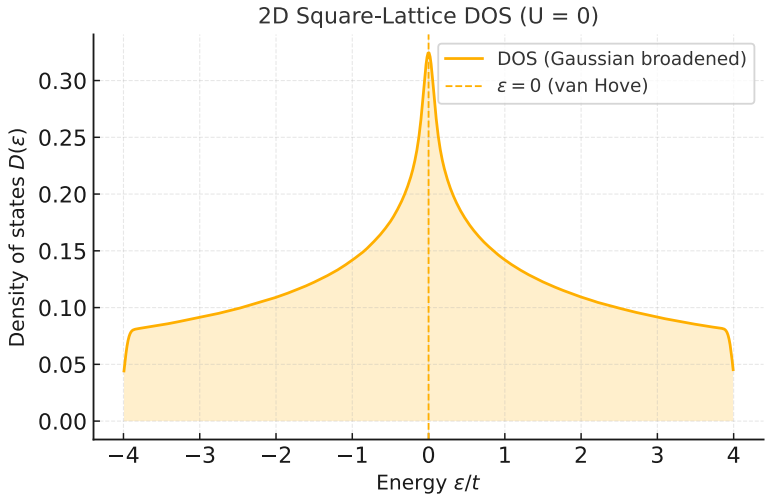

Figure 9: Density of states for the non-interacting 2-D square-lattice Hubbard model. A Gaussian broadening $\sigma = 0.05\,t$ smooths the histogram while retaining the logarithmic van-Hove singularity at $\epsilon = 0$ (dashed line).

The corresponding spectral function is:

$$A(\mathbf{k}, \omega) = 2\pi\delta(\omega - \xi_{\mathbf{k}}) \tag{63}$$

This reflects the non-interacting nature of the system: the spectral weight is sharply localized at the quasiparticle energy $\xi_{\mathbf{k}}$.

4 Mean-Field Treatment of the Interaction Term

A standard first approximation to the full Hubbard Hamiltonian is to treat one term as a perturbation around the solvable limit of the other. Here, we begin from the non-interacting limit H_0, assuming that $U < t$ but still sufficiently strong to qualitatively modify the properties of the free Fermi gas. We apply a mean-field approximation to capture the effects of interactions.

We rewrite the Hubbard Hamiltonian as $H = H_0 + H_1$, where

$$H_0 = \sum_{\mathbf{k},\sigma} \xi_{\mathbf{k}} c^\dagger_{\mathbf{k},\sigma} c_{\mathbf{k},\sigma} \tag{64}$$

$$H_1 = U \sum_j (n_{j\uparrow} - \frac{1}{2})(n_{j\downarrow} - \frac{1}{2}) = \sum_j \{U n_{j\uparrow} n_{j\downarrow} - \frac{U}{2}(n_{j\uparrow} + n_{j\downarrow})\} + \frac{U}{2} N \tag{65}$$

The last term is an overall shift in energy; we ignore it, and we redefine μ as $\tilde{\mu} := \mu + \frac{U}{2}$, which goes into $\xi_{\mathbf{k}}$ as $\tilde{\xi}_{\mathbf{k}} = \epsilon_{\mathbf{k}} - \tilde{\mu}$. We assume that fluctuations in the local occupation number $\langle n_{j,\sigma} \rangle$ are small, allowing us to linearize the interaction term around its mean value. The Mean-Field Hubbard Hamiltonian is thus

$$H_{MF} = \sum_{\mathbf{k},\sigma} \tilde{\xi}_{\mathbf{k}} c^\dagger_{\mathbf{k},\sigma} c_{\mathbf{k},\sigma} + U \sum_j (n_{j,\uparrow} \langle n_{j,\downarrow} \rangle + n_{j,\downarrow} \langle n_{j,\uparrow} \rangle) \tag{66}$$

In half-filled materials ($\rho = 1$), antiferromagnetic (AFM) order is experimentally observed. To capture this, we introduce a staggered magnetization m_j defined as

$$m_j = \frac{1}{2}[\langle n_{j,\uparrow} \rangle - \langle n_{j,\downarrow} \rangle](-1)^{r+s} = m(-1)^{r+s} \tag{67}$$

where m is the sublattice magnetization density, the amplitude of the staggered spin pattern, and $\mathbf{R_j} = a(r, s)$. This definition is equivalent to assuming a magnetic order with a wave vector $\mathbf{q} = (\pi, \pi)/a$, corresponding to the nesting vector we have met before. This means that the magnetic pattern varies in space with periodicity described by $\mathbf{q}$, since

$$S^z_j = m(-1)^{r+s} = m e^{i\mathbf{q}.\mathbf{R_j}} = m e^{i\pi(r+s)} \tag{68}$$

and $e^{i\mathbf{q}.\mathbf{R_j}} = \pm 1$ depending on the sub-lattice $\mathbf{R_j}$ belongs to. We parameterize $\langle n_{j,\uparrow} \rangle$ and $\langle n_{j,\downarrow} \rangle$ in terms of m, as

$$\langle n_{j,\uparrow} \rangle = \frac{1}{2} + (-1)^{r+s} m \tag{69}$$

$$\langle n_{j,\downarrow} \rangle = \frac{1}{2} - (-1)^{r+s} m \tag{70}$$

When $m = 0$, $\langle n_{j,\uparrow} \rangle = \langle n_{j,\downarrow} \rangle = \frac{1}{2}$, and the system is paramagnetic. Whereas in the other extreme, we have $\langle n_j \rangle = \langle n_{j,\uparrow} \rangle = 1$ for, say, $r + s$ is even, and $\langle n_j \rangle = \langle n_{j,\downarrow} \rangle = -1$ for $r + s$ is odd, and we get a perfect AFM order. Focusing on a single sublattice, the AFM order effectively doubles the unit cell and leads to a $\pi/4$ rotation of the reciprocal lattice relative to the original square lattice. The old, primitive, and reciprocal lattice vectors were

$$\mathbf{a_1} = a(1, 0),\ \mathbf{a_2} = a(0, 1) \tag{71}$$

$$\mathbf{b_1} = \frac{2\pi}{a}(1, 0),\ \mathbf{b_2} = \frac{2\pi}{a}(0, 1) \tag{72}$$

In the new, $\frac{\pi}{4}$ rotated square, lattice, we have

$$\mathbf{a'_1} = a(1, -1),\ \mathbf{a'_2} = a(1, 1) \tag{73}$$

$$\mathbf{b'_1} = \frac{\pi}{a}(1, -1),\ \mathbf{b'_2} = \frac{\pi}{a}(1, 1) = \mathbf{q} \tag{74}$$

This means that the new Brillouin Zone F is half the size of the old one. Substituting into H_{MF}, we get

$$H^{AF}_{MF} = \sum_{\mathbf{k},\sigma} \tilde{\xi}_{\mathbf{k}} c^\dagger_{\mathbf{k},\sigma} c_{\mathbf{k},\sigma} + \sum_{j,\sigma} \frac{U}{2}[1 - 2m\sigma(-1)^{r+s}] c^\dagger_{j,\sigma} c_{j,\sigma} \tag{75}$$

$$H^{AF}_{MF} = \sum_{\mathbf{k},\sigma} \tilde{\xi}_{\mathbf{k}} c^\dagger_{\mathbf{k},\sigma} c_{\mathbf{k},\sigma} - mU \sum_{j,\sigma} \sigma(-1)^{r+s} c^\dagger_{j,\sigma} c_{j,\sigma} + \frac{U}{2} \sum_j n_j \tag{76}$$

The last term cancels the existing $\frac{U}{2}$ shift in the chemical potential, now reads $\tilde{\mu} = \mu$, and $\tilde{\xi}_{\mathbf{k}} = \xi_{\mathbf{k}}$. H^{AF}_{MF} now reads

$$H^{AF}_{MF} = \sum_{\mathbf{k},\sigma} \xi_{\mathbf{k}} c^\dagger_{\mathbf{k},\sigma} c_{\mathbf{k},\sigma} - mU \sum_{j,\sigma} \sigma e^{i\mathbf{q}.\mathbf{R_j}} c^\dagger_{j,\sigma} c_{j,\sigma} \tag{77}$$

Using the definitions in equations (52) and (54), with $\mathbf{k} \in 1^{st}$ BZ, we see that the effect of $e^{i\mathbf{q}.\mathbf{R_j}}$ is nesting the $\mathbf{k}$ vectors, and

$$H_{MF}^{AF} = \sum_{\mathbf{k},\sigma} \xi_{\mathbf{k}} c_{\mathbf{k},\sigma}^{\dagger} c_{\mathbf{k},\sigma} - mU \sum_{\mathbf{k},\sigma} \sigma c_{\mathbf{k}+\mathbf{q},\sigma}^{\dagger} c_{\mathbf{k},\sigma} \tag{78}$$

$$= \sum_{\mathbf{k},\sigma} \epsilon_{\mathbf{k}} c_{\mathbf{k},\sigma}^{\dagger} c_{\mathbf{k},\sigma} - \mu \sum_{\mathbf{k},\sigma} n_{\mathbf{k},\sigma} - mU \sum_{\mathbf{k},\sigma} \sigma c_{\mathbf{k}+\mathbf{q},\sigma}^{\dagger} c_{\mathbf{k},\sigma} \tag{79}$$

The effect of the third term is to scatter electrons from state $\mathbf{k}$ to $\mathbf{k}+\mathbf{q}$ without flipping the spin. By reducing the Hamiltonian calculation within the reduced Brillouin Zone, we can diagonalize this Hamiltonian, details in Appendix A :

$$H_{MF,\mu=0}^{AF} = \sum_{\mathbf{k}\in F,\sigma} E_{\mathbf{k}} \{ d_{\mathbf{k},\sigma}^{\dagger} d_{\mathbf{k},\sigma} - d_{\mathbf{k}+\mathbf{q}\sigma}^{\dagger} d_{\mathbf{k}+\mathbf{q}\sigma} \} \tag{80}$$

The resulting model describes a two-band insulator with an energy gap of $2\Delta = 2mU$ at half-filling, where $E_{\mathbf{k}}^{1(2)} = \pm\sqrt{\epsilon_{\mathbf{k}}^2 + \Delta^2} = \pm E_{\mathbf{k}}$, capturing the insulating behavior observed in the parent compounds of cuprates. We have assumed an AFM order with m magnetisation; now, we calculate m self-consistently. First, we calculate it from $H_{MF,\mu=0}^{AF}$ and then equate it to $m = \frac{1}{N}\sum_j \frac{(-1)^j}{2}[\langle n_{j,\uparrow}\rangle - \langle n_{j,\downarrow}\rangle]$. Starting from

$$n_{j,\sigma} = c_{j,\sigma}^{\dagger} c_{j,\sigma} = \frac{1}{N} \sum_{\mathbf{k},\mathbf{k}'} e^{-i(\mathbf{k}-\mathbf{k}').\mathbf{R_j}} c_{\mathbf{k},\sigma}^{\dagger} c_{\mathbf{k}',\sigma} \tag{81}$$

We get

$$1 = \frac{U}{N} \sum_{\mathbf{k}\in F} \frac{1}{E_{\mathbf{k}}} \tag{82}$$

Going to the continuum limit, i.e. $N \to \infty$,

$$1 = U(\frac{a}{2\pi})^2 \int_F \frac{dk^2}{\sqrt{\epsilon_{\mathbf{k}}^2 + \Delta^2}} \tag{83}$$

Going to polar coordinates, changing variables from k to ϵ, where as $|\mathbf{k}|$ goes from $(0,0)$ to $(\frac{\pi}{2a}, \frac{\pi}{2a})$, $\epsilon \in (-4t, 0)$, and introducing the density of states $\rho(\epsilon)$, we get

$$1 = U \int_{-4t}^{0} \rho(\epsilon) \frac{d\epsilon}{\sqrt{\epsilon^2 + \Delta^2}} \tag{84}$$

changing variables again $\epsilon \longrightarrow -\epsilon$ with $\rho(-\epsilon) = \rho(\epsilon)$, recall that we have two bands symmetric around $\epsilon = 0$, we get

$$1 = U \int_{0}^{4t} \rho(\epsilon) \frac{d\epsilon}{\sqrt{\epsilon^2 + \Delta^2}} \tag{85}$$

In the weak-coupling limit ($U \ll t$) we assume a small but finite order parameter Δ. Because the two-dimensional density of states diverges logarithmically,

$$\rho(\epsilon) \;\approx\; \frac{1}{2\pi^2 t}\, \ln\frac{8t}{|\epsilon|},$$

the k-space integral that enters the mean-field gap equation is dominated by energies $|\epsilon| \lesssim \Delta$:

$$\frac{1}{U} \;=\; \int_{-W}^{W} \frac{\rho(\epsilon)\, d\epsilon}{2\sqrt{\epsilon^2 + \Delta^2}} \;\simeq\; \frac{1}{2\pi^2 t}\, \ln\frac{16t}{\Delta},$$

where $W = 4t$ is the half-bandwidth. Solving for Δ yields

$$\boxed{\Delta \;=\; 16\, t\, \exp\!\Big[-2\pi\sqrt{\tfrac{t}{U}}\Big]}$$

(the numerical prefactor depends on the ultraviolet cut-off and is therefore non-universal). As $U \to 0$ the gap collapses, but the square-root exponent makes the approach much slower than the usual $\exp(-\text{const}\; t/U)$ found in

metals with a finite $\rho(0)$. Consequently, even weak interactions favour antiferromagnetic order on the square lattice. For the opposite situation, $U >> t$, and $\Delta >> t$ dominates the integrand denominator. Thus, we find approximately

$$1 = \frac{U}{\Delta}\int_0^{4t} \rho(\epsilon)d\epsilon \tag{86}$$

But since $\int_{-4t}^{4t} \rho(\epsilon)d\epsilon = 1$, then $\Delta = U/2$. As U increases further, Δ approaches U, consistent with the Mott gap identified in the single-site Hubbard model.

Conclusion

The mean-field treatment of the Hubbard model at half-filling reveals an antiferromagnetic insulating ground state induced by electron–electron interactions. In the weak-coupling regime, the gap Δ opens exponentially with $\sqrt{t/U}$, characterizing a Slater insulator driven by Fermi surface nesting. In contrast, the strong-coupling limit leads to a Mott-like gap that scales linearly with U, connecting this analysis with the atomic limit previously studied. This unifies the weak- and strong-coupling pictures and reinforces the interpretation of parent cuprates as Mott insulators with antiferromagnetic order—a central theme that motivates our subsequent DMFT study.

5 Perturbative Treatment of the Kinetic Energy Term

We now consider the opposite limit, $U \gg t$, treating the kinetic energy term as a perturbation to the dominant interaction term. At half-filling, $\mu = 0$,

$$H = U\sum_j (n_{j\uparrow} - \frac{1}{2})(n_{j\downarrow} - \frac{1}{2}) - t\sum_{\langle i,j\rangle\sigma}(c^\dagger_{j\sigma}c_{i\sigma} + c^\dagger_{i\sigma}c_{j\sigma}) = H^U + H^1 \tag{87}$$

To capture the essential physics in a tractable way, we restrict our attention to the two-site Hubbard model. While simplified, this model illustrates the key ideas clearly. A more complete, though slightly different, treatment can be found in [18]. We now have

$$H^U = U\sum_j^2 (n_{j\uparrow} - \frac{1}{2})(n_{j\downarrow} - \frac{1}{2}) \tag{88}$$

$$H^1 = -t\sum_\sigma (c^\dagger_{j\sigma}c_{i\sigma} + c^\dagger_{i\sigma}c_{j\sigma}) \tag{89}$$

5.1 Hubbard Subbands

Before proceeding, we briefly introduce the concept of Hubbard subbands via an intuitive argument inspired by ref. [18]. A rigorous derivation is given in the third paper of Hubbard's original series. Consider an N-site Hubbard lattice at $t = 0$: the system consists of N copies of the single-site energy levels from equation (36), which we reinterpret as single-electron energy levels. If there is only one electron in the system, it occupies a level with energy ϵ_{at}. If a second electron is added to the same site, the double occupancy is interpreted as one electron in ϵ_{at}, and the second in $\epsilon_{at} + U$, as illustrated in Fig. 10a.

Now, assume we have $N + 1$ electrons and still $t = 0$. The ground states consist of N electrons occupying the lower levels at ϵ_{at}, while the additional electron can occupy any of the $\epsilon_{at} + U$ levels. Suppose the electrons in the lower levels are all spin-down, and the one in the upper level is spin-up. When the hopping term is introduced, the extra electron can delocalize across its z nearest neighbors, effectively broadening the upper level into a band of width $\sim 2zt$. Similarly, if we now consider only $N - 1$ electrons in the lower levels and examine the motion of a hole, the lower level also broadens into a band of width $\sim 2zt$. This leads to the formation of two Hubbard subbands, as shown in 10b.

5.2 Effective Hamiltonian

We look for an effective Hamiltonian that describes the physics in the lowest Hubbard subband, namely the one with no doubly occupied sites.

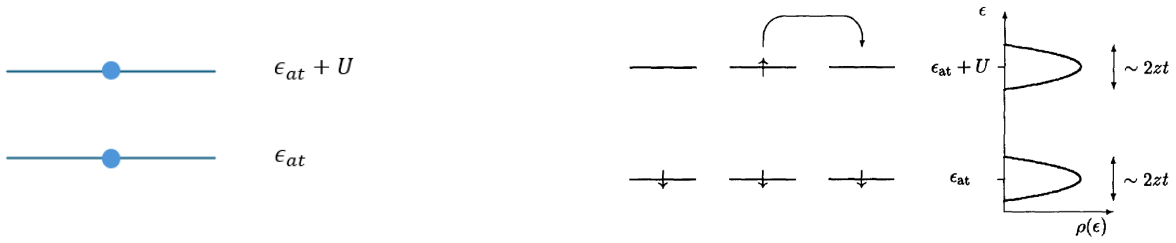

(a) Single-electron energy levels representation of the Hubbard Hamiltonian in the single-site limit.

(b) Formation of Hubbard subbands as broadening of the single-electron energy levels due to hopping, from [18].

Figure 10

We are treating the kinetic energy as a perturbation, so we first divide it into three parts depending on how the parts change the total number of doubly occupied sites, H^0, H^-, H^+. To do so, we introduce the projection operators on the four single-site states defined as

$$\hat{P}_{j0} = |0\rangle_j \langle 0| = (1 - n_{j\uparrow})(1 - n_{j\downarrow}) \tag{90}$$

$$\hat{P}_{j\sigma} = n_{j\sigma}(1 - n_{j-\sigma}) \tag{91}$$

$$\hat{P}_{jd} = |d\rangle_j \langle d| = n_{j\uparrow} n_{j\downarrow} \tag{92}$$

$$\hat{P}_{j0} + \hat{P}_{j\uparrow} + \hat{P}_{j\downarrow} + \hat{P}_{jd} = \mathbb{I}$$

Using these operators, we can identify the different processes in H_1. For example, consider the case where site 2 has an $\uparrow$ electron and site 1 has an $\downarrow$ electron. The operator $c^\dagger_{1\uparrow} c_{2\uparrow}$ would increase the number of doubly occupied sites by one by transferring the $\uparrow$ electron from site 2 to site 1, and to single out this process we have the following term,

$$\hat{P}_{1d} c^\dagger_{1\uparrow} c_{2\uparrow} \hat{P}_{2\uparrow} \tag{93}$$

Collecting all terms that increase the number of d sites, we get

$$H^+ = -t \sum_\sigma \left\{ \hat{P}_{1d} c^\dagger_{1\sigma} c_{2\sigma} \hat{P}_{2\sigma} + \hat{P}_{2d} c^\dagger_{2\sigma} c_{1\sigma} \hat{P}_{1\sigma} \right\} \tag{94}$$

Similarly, we have

$$H^- = -t \sum_\sigma \left\{ \hat{P}_{1\sigma} c^\dagger_{1\sigma} c_{2\sigma} \hat{P}_{2d} + \hat{P}_{2\sigma} c^\dagger_{2\sigma} c_{1\sigma} \hat{P}_{1d} \right\} \tag{95}$$

$$H^0 = -t \sum_\sigma \left\{ \hat{P}_{1d} c^\dagger_{1\sigma} c_{2\sigma} \hat{P}_{2d} + \hat{P}_{2\sigma} c^\dagger_{2\sigma} c_{1\sigma} \hat{P}_{1\sigma} + H.C. \right\} \tag{96}$$

The total Hamiltonian is $H = H^0 + H^+ + H^- + H^U$, where H^+, H^-, and H^0 increases, decreases and does not change the number of doubly occupied sites, respectively. Our goal is to eliminate, at least to leading order in t, the transitions between the low-energy and high-energy Hubbard subbands. We use a kind of Schrieffer–Wolff unitary transformation S to go to a new basis where this is possible. It is as follows :

$$H_{eff} = e^{iS} H e^{-iS} \tag{97}$$

$$S = -\frac{i}{U}(H^+ - H^-) \tag{98}$$

This leads to

$$H_{eff} = H^0 + H^U + \frac{1}{U}[H^+, H^-] \tag{99}$$

Recall that we are considering the half-filling case where the lowest subband, in this two-site Hubbard Hamiltonian, contains one electron at each site. In this case, there are no double occupations, and of course, we cannot decrease them.

Thus there are no contributions from H^U and H^-. Furthermore, there is no hopping that conserves the number of double occupied sites, i.e. no contributions from H^0 as well. We end up with

$$H_{eff} = -\frac{1}{U} H^- H^+ \tag{100}$$

To understand the meaning of our result, recall that in the half-filled two-site Hubbard model, the full Hilbert space is spanned by

$$|\uparrow,\uparrow\rangle, |\downarrow,\downarrow\rangle, |\uparrow,\downarrow\rangle, |\downarrow,\uparrow\rangle, |\uparrow\uparrow,0\rangle, |0,\uparrow\uparrow\rangle, |\downarrow\downarrow,0\rangle, |0,\downarrow\downarrow\rangle \tag{101}$$

with the notation $|\text{site 1}, \text{site 2}\rangle$. Now that we have used a unitary transformation to go to a different basis in which the lowest Hubbard sub-band, $|\uparrow,\uparrow\rangle, |\downarrow,\downarrow\rangle, |\uparrow,\downarrow\rangle, |\downarrow,\uparrow\rangle$ doesn't couple to the higher ones, $|\uparrow\uparrow,0\rangle, |0,\uparrow\uparrow\rangle, |\downarrow\downarrow,0\rangle, |0,\downarrow\downarrow\rangle$. In the original basis, H_{eff} describes virtual transitions into higher-energy doubly occupied states and back. In the transformed basis—restricted to the singly occupied subspace—these virtual processes manifest as effective spin exchange, i.e., spin fluctuations. To understand the effect of H_{eff}, we calculate the matrix elements of H_{eff} in the lowest sub-band, with the convention that

$$|\uparrow,\downarrow\rangle = c^\dagger_{1\uparrow} c^\dagger_{2\downarrow} |0,0\rangle \tag{102}$$

$$|\uparrow\downarrow,0\rangle = c^\dagger_{1\uparrow} c^\dagger_{1\downarrow} |0,0\rangle \tag{103}$$

we get

$$H_{eff} |\uparrow,\uparrow\rangle = H_{eff} |\downarrow,\downarrow\rangle = 0 \tag{104}$$

$$\langle\uparrow,\downarrow| H_{eff} |\uparrow,\downarrow\rangle = \langle\downarrow,\uparrow| H_{eff} |\downarrow,\uparrow\rangle = -2\frac{t^2}{U} \tag{105}$$

$$\langle\uparrow,\downarrow| H_{eff} |\downarrow,\uparrow\rangle = \langle\downarrow,\uparrow| H_{eff} |\uparrow,\downarrow\rangle = +2\frac{t^2}{U} \tag{106}$$

The factor of 2 arises because the electron can be removed from either site first—the two sequences are indistinguishable and therefore add coherently, and the difference of sign is because we have to pay attention to the convention used in defining the states. There are several ways to proceed. One may write H_{eff} in terms of creation and annihilation operators and then express it using

$$c^\dagger_\sigma c_\sigma = \frac{1}{2} + \sigma S^z \tag{107}$$

$$c^\dagger_\sigma c_{-\sigma} = S^x + i\sigma S^y \tag{108}$$

In Appendix B, we present a first-quantization approach, which leads to

$$H_{eff} = 4\frac{t^2}{U}\Big\{\mathbf{S}_1.\mathbf{S}_2 - \frac{\mathbb{I}}{4}\Big\} \tag{109}$$

This is the Heisenberg Hamiltonian, which favors an AFM order.

Conclusion

Why the unitary transformation achieves a projection. We choose the Schrieffer–Wolff generator $S = -\frac{i}{U}(H^+ - H^-)$ so that, to first order in t/U, the off-diagonal blocks that couple the no-doublon subspace P to the doublon subspace Q cancel: $P\big(H_t + i[S, H_U]\big)Q = 0$. Here one uses $[H^+, H_U] = -U\, H^+$ and $[H^-, H_U] = +U\, H^-$. The transformed Hamiltonian $H_{\text{eff}} = e^{iS} H e^{-iS} = PHP + \frac{1}{U}[H^+, H^-] + \mathcal{O}(t^3/U^2)$ is thus block-diagonal up to $\mathcal{O}(t/U)$; we can safely *project* onto P (the singly–occupied sector) and obtain the low-energy Heisenberg super-exchange $J = 4t^2/U$.

In the strong-coupling limit of the Hubbard model at half-filling, where $U \gg t$, perturbation theory reveals an effective low-energy theory governed by spin degrees of freedom. Virtual hopping processes between neighboring sites induce an antiferromagnetic exchange interaction described by the Heisenberg Hamiltonian, with coupling constant $J = 4t^2/U$. This result connects the Hubbard model to quantum magnetism and shows that in the strong-coupling regime, Mott insulating behavior is accompanied by emergent spin order.

6 Dynamical Mean Field Theory (DMFT)

Why do we need a more sophisticated method like DMFT, if we already have two approximate solutions—the weak-coupling mean-field and strong-coupling perturbation approaches? In the weak-coupling limit, we treated interactions at the mean-field level, obtaining antiferromagnetic ordering and an interaction-induced gap — a so-called Slater insulator. However, this approach provides an insulating phase only if an antiferromagnetic order parameter sets in. Now, correlated materials like the copper oxides (see Fig. 2b) still display insulating behavior at temperatures above the antiferromagnetic transition, a Mott paramagnetic insulator, which cannot be accounted for within the antiferromagnetic scenario. Conversely, in the strong-coupling limit, perturbation theory around $U \gg t$ produces an effective Heisenberg model describing localized spins and antiferromagnetic correlations. While this captures the essence of the Mott insulating regime, it cannot describe itinerant or metallic behavior.

Both approaches miss the rich physics of the intermediate coupling regime, where interactions are strong enough to induce correlations, but not strong enough to fully localize electrons. Crucially, neither method retains the *frequency dependence* of electron self-energy, which governs lifetime, spectral weight transfer, and the emergence of Hubbard bands. To overcome these limitations, we now turn to **Dynamical Mean-Field Theory (DMFT)** [19] — a non-perturbative approach that treats local quantum dynamics exactly while approximating spatial fluctuations. It allows us to track the evolution from weak to strong coupling in a unified framework, capturing both metallic and insulating behavior on equal footing. We now develop the DMFT formalism, which, unlike earlier approximations, can treat the full Hubbard Hamiltonian across all coupling regimes—a method analogous to the classical mean-field treatment of the Ising model or Density Functional Theory (DFT).

Following ref. [20], the idea is to represent the system by a local quantity coupled to an effective bath; a pictorial representation is in Fig. 11. In the limit of infinite spatial dimension (i.e. high lattice coordinator number), we can

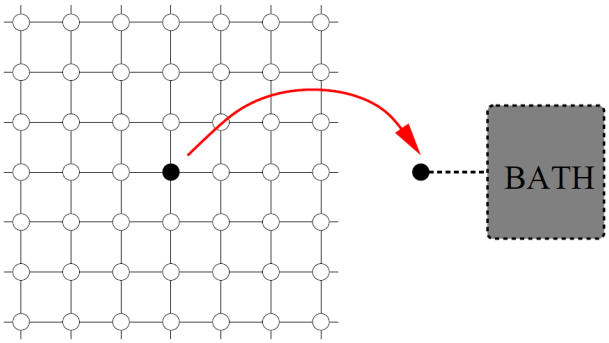

Figure 11: Pictorial representation of DMFT, from [20]

exactly reformulate the full Hubbard model as a self-consistent Anderson Impurity Model (AIM) [21], where a single interacting site (the impurity) is coupled to a non-interacting bath. Here, the physical sites are denoted by the "c" operators, and bath sites by the "a" operators:

$$H = -t \sum_{\langle i,j\rangle\sigma} (c^\dagger_{j\sigma} c_{i\sigma} + c^\dagger_{i\sigma} c_{j\sigma}) + U \sum_j n_{j\uparrow} n_{j\downarrow} + (\epsilon_{at} - \mu) \sum_{j\sigma} n_{j\sigma} \tag{110}$$

$$\Updownarrow \tag{111}$$

$$H_{AIM} = H_{atom} + H_{bath} + H_{coupling} \tag{112}$$

$$H_{AIM} = U n^c_\uparrow n^c_\downarrow + (\epsilon_{at} - \mu)(n^c_\uparrow + n^c_\downarrow) + \sum_{l\sigma} \tilde{\epsilon}_l a^\dagger_{l\sigma} a_{l\sigma} + \sum_{l\sigma} V_l (a^\dagger_{l\sigma} c_\sigma + c^\dagger_\sigma a_{l\sigma}) \tag{113}$$

Usually, in the single-band Hubbard model, we put the single-electron atomic level energy $\epsilon_{at} := 0$ since, in the Grand Canonical Ensemble, everything depends on μ. Here we explicitly write it down, anticipating the representation by an AIM. In both models, we have the same interaction energy U, chemical potential μ, and single-electron atomic level energy $\epsilon_{at} := 0$. The parameters $\tilde{\epsilon}_l$ and V_l are chosen in such a way that the impurity's Green's function coincides with the local Green's function of the Hubbard Hamiltonian, i.e.

$$G^{Hub}_{loc}(i\omega_n) \equiv G^{AIM}_{imp}(i\omega_n) \tag{114}$$

We emphasize again that this is an ***exact*** representation in the infinite-dimensional limit; there are no approximations yet that are applied in the case of finite-dimensional real materials. Using effective action functional integral formalism, we can see that the parameters $\tilde{\epsilon_l}$ and V_l in the AIM enter only through a hybridization function Δ (not shown here), by integrating out the bath degrees of freedom we get the effective action for the impurity orbital only as

$$S_{eff} = -\int_0^\beta d\tau \int_0^\beta d\tau' \sum_\sigma c_\sigma^\dagger(\tau)\mathcal{G}_0^{-1}(\tau-\tau')c_\sigma(\tau') + U\int_0^\beta d\tau n_\uparrow(\tau)n_\downarrow(\tau) \tag{115}$$

$$\mathcal{G}_0^{-1}(i\omega_n) = i\omega_n + \mu - \epsilon_{at} - \Delta(i\omega_n) \tag{116}$$

$$\Delta(i\omega_n) = \sum_l \frac{|V_l|^2}{i\omega_n - \tilde{\epsilon_l}} \tag{117}$$

$\mathcal{G}_0$ plays the role of a bare Green's function for the effective action S_{eff}, and it is called the Weiss dynamical field in analogy with the classical mean-field theory. From the interacting Green's function of S_{eff}, $G_{imp} \equiv -\langle T_\tau c(\tau)c^\dagger(\tau')\rangle_{S_{eff}}$. We define a local self-energy Σ_{imp} using Dyson's equation:

$$\Sigma_{imp}(i\omega_n) \equiv \mathcal{G}_0^{-1}(i\omega_n) - G_{imp}^{-1}(i\omega_n) \tag{118}$$

$$= i\omega_n + \mu - \epsilon_{at} - \Delta(i\omega_n) - G_{imp}^{-1}(i\omega_n) \tag{119}$$

Going back to the original Hubbard Hamiltonian, the interacting Green's function is given by

$$G(\mathbf{k}, i\omega_n) = \frac{1}{i\omega_n + \mu - \epsilon_{at} - \epsilon_\mathbf{k} - \Sigma(\mathbf{k}, i\omega_n)} \tag{120}$$

where $\epsilon_\mathbf{k}$ is the original lattice dispersion of the hopping part. The key property in the infinite-dimensional limit is that the self-energy is purely local [21], so that its $\mathbf{k}$ dependence can be dropped out. We can therefore identify the lattice self-energy with that of the impurity model:

$$\Sigma(i\omega_n) = \Sigma_{imp}(i\omega_n) \tag{121}$$

In real systems, this correspondence must be considered as an approximation, which can work very well in some high coordination materials [22]. The lattice Green's function simplifies to:

$$G_{loc}(i\omega_n) = \sum_\mathbf{k} G(\mathbf{k}, i\omega_n) = \sum_\mathbf{k} \frac{1}{i\omega_n + \mu - \epsilon_{at} - \epsilon_\mathbf{k} - \Sigma(\mathbf{k}, i\omega_n)} \tag{122}$$

$$= \sum_\mathbf{k} \frac{1}{i\omega_n + \mu - \epsilon_{at} - \epsilon_\mathbf{k} - \Sigma_{imp}(i\omega_n)} \tag{123}$$

Using equation 119, we have :

$$G_{loc}(i\omega_n) = \sum_\mathbf{k} \frac{1}{\Delta(i\omega_n) + G_{imp}^{-1}(i\omega_n) - \epsilon_\mathbf{k}} \equiv G_{imp}(i\omega_n) \tag{124}$$

We have therefore established a self-consistent closed equation for $G_{imp}(i\omega_n)$. Finally, introducing the non-interacting density of states $D(\epsilon) = \sum_\mathbf{k} \delta(\epsilon - \epsilon_\mathbf{k})$, we can express the self-consistency condition as:

$$\int \frac{D(\epsilon)}{\Delta(i\omega_n) + G^{-1}(i\omega_n) - \epsilon} d\epsilon \; = \; G(i\omega_n) \tag{125}$$

6.1 The DMFT Loop

In practical implementations, the DMFT algorithm begins with an *initial guess* for the Weiss field $\mathcal{G}_0(i\omega_n)$, which acts as the non-interacting Green's function for the impurity problem. Using this guess, one solves the impurity problem—defined by the effective action S_{eff}—with an *impurity solver* to obtain the interacting impurity Green's function $G_{imp}(i\omega_n)$. From this, the local self-energy $\Sigma_{imp}(i\omega_n)$ is computed via Dyson's equation: (118). This self-energy is then used to compute the local lattice Green's function $G_{loc}(i\omega_n)$ via the self-consistency equation (125). An updated Weiss field is then reconstructed using the identity:

$$\mathcal{G}_{0,new}^{-1} = G_{loc}^{-1} + \Sigma_{imp} \tag{126}$$

This updated $\mathcal{G}_0$ is passed again to the impurity solver, and the procedure is iterated until convergence is reached—typically when G_{imp} (and Σ_{imp}) stop changing appreciably between iterations. A schematic illustration of the DMFT loop is shown in Fig. 12

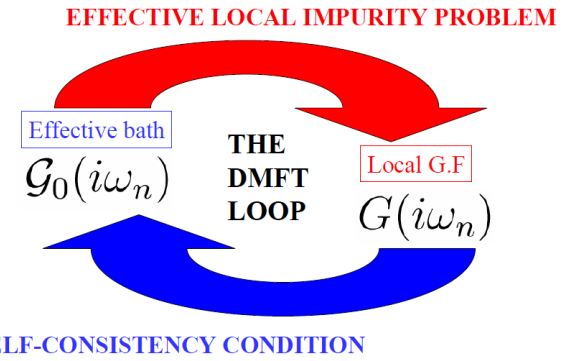

Figure 12: Pictorial representation of the DMFT loop, from [20]

6.2 Landau's Fermi Liquid Theory

The central idea of Landau's Fermi liquid theory is that the low-energy excitations of an interacting electron system can be described in terms of long-lived, weakly interacting *quasiparticles*, which resemble the excitations of a free Fermi gas. Starting from the ground state $|G\rangle$ of the non-interacting Fermi gas (with a well-defined Fermi surface), we adiabatically switch on interactions to reach the ground state $|\tilde{G}\rangle$ of the interacting system. We assume that the Fermi surface persists under this evolution. If not, we assume $|\tilde{G}\rangle$ can still be reached from an excited state of the non-interacting system.

Now consider an excited state with an electron (hole) at $\mathbf{k} > \mathbf{k}_F$ (resp. $\mathbf{k} < \mathbf{k}_F$), the state reached by adiabatically continuing this state is called a quasi-particle(hole) state. Each particle (or hole) excitation of the non-interacting system evolves into a corresponding quasiparticle (or quasihole) excitation of the interacting system, provided that the excitation does not decay during the adiabatic switching. This gives a one-to-one mapping between excitations:

$$|G\rangle \xrightarrow{\textit{Adiabatic Continuation}} |\tilde{G}\rangle \tag{127}$$

$$c^\dagger_{\mathbf{k}>\mathbf{k}_F}|G\rangle \xrightarrow{\textit{Adiabatic Continuation}} |\tilde{1}\rangle \tag{128}$$

$$\vdots$$

For this continuation to be valid, the turning-on time of the interaction must be neither too long (to avoid decay) nor too short (to maintain adiabaticity). Near the Fermi surface ($k \to k_F$), the phase space for scattering processes becomes vanishingly small. As a result, quasiparticles become increasingly long-lived. In the exact limit $k = k_F$, their lifetime diverges, justifying the description of low-energy excitations in terms of well-defined quasiparticles.

To formalize the quasiparticle picture, we examine the retarded Green's function and its corresponding spectral function.

$$G^R(\mathbf{k},\omega) = \frac{1}{\omega - \xi_\mathbf{k} - \Re\Sigma^R(\mathbf{k},\omega) - i\Im\Sigma^R(\mathbf{k},\omega)} \tag{129}$$

$$A(\mathbf{k},\omega) = -\frac{1}{\pi}\Im G^R(\mathbf{k},\omega) = -\frac{1}{\pi}\frac{\Im\Sigma^R(\mathbf{k},\omega)}{[\omega - \xi_\mathbf{k} - \Re\Sigma^R(\mathbf{k},\omega)]^2 + [\Im\Sigma^R(\mathbf{k},\omega)]^2} \tag{130}$$

where $\Im\Sigma^R(\mathbf{k},\omega) < 0$ so that $A^R(\mathbf{k},\omega) > 0$ as it should. Since $\Im\Sigma^R < 0$, this ensures $A > 0$, as required for a probability density. Near the Fermi surface and for small frequencies, we expand the real part of the self-energy as:

$$\Re\Sigma^R(\mathbf{k},\omega) \approx \Re\Sigma^R(\mathbf{k},0) + \left.\frac{d\Re\Sigma^R}{d\omega}\right|_{\omega=0}\omega + \mathcal{O}(\omega^2) \tag{131}$$

Substituting this into the Green's function and defining:

$$Z = \left[1 - \left.\frac{d\Re\Sigma^R}{d\omega}\right|_{\omega=0}\right]^{-1}, \quad \tilde{\xi}_\mathbf{k} = Z\left[\xi_\mathbf{k} + \Re\Sigma^R(\mathbf{k},0)\right] \tag{132}$$

we obtain:

$$A^R(\mathbf{k},\omega) \approx \frac{Z}{\pi}\frac{-Z\Im\Sigma^R(\mathbf{k},\omega)}{[\omega-\tilde{\xi}_{\mathbf{k}}]^2+[Z\Im\Sigma^R(\mathbf{k},\omega)]^2} \tag{133}$$

This is a Lorentzian peak centered at $\tilde{\xi}_{\mathbf{k}}$, with width $Z|\Im\Sigma^R|$ and spectral weight Z. Taking the limit $\Im\Sigma^R \to 0$, the quasiparticle becomes infinitely long-lived and the spectral function reduces to:

$$A(\mathbf{k},\omega) = Z\delta(\omega-\tilde{\xi}_{\mathbf{k}}) \tag{134}$$

This delta function describes a stable quasiparticle with renormalized dispersion and weight $0 < Z < 1$, capturing the essence of Landau's Fermi liquid theory.

We could've also expanded $\Im\Sigma^R(\mathbf{k},\omega)$ around $\omega = 0$, which leads to

$$\Im\Sigma^R(\mathbf{k},\omega) \approx \omega^2 + \mathcal{O}(\omega^3) \tag{135}$$

$$G^R(\mathbf{k},\omega) \approx \frac{Z}{\omega - Z[\xi_{\mathbf{k}} + \Re\Sigma^R(\mathbf{k},\omega=0)]} \tag{136}$$

Doing so assumes infinite lifetime of the quasiparticles, where now $\omega \equiv \omega + i\eta$. Then, using equation (46), and taking the imaginary part, we get

$$A^R(\mathbf{k},\omega) = Z\delta(\omega-\tilde{\xi}_{\mathbf{k}}) \tag{137}$$

Same as before. This picture of a renormalized, long-lived quasiparticle peak—emerging from a background of incoherent excitations—is central to the interpretation of spectral functions in DMFT. It allows us to distinguish between metallic (coherent quasiparticles are well defined) and insulating (incoherent or gapped, where quasiparticles are not well defined anymore) regimes across interaction strengths.

6.3 The IPT Solver

We now introduce a simple yet insightful solver for the impurity model — Iterated Perturbation Theory (IPT). Although approximate, IPT captures important physics and is computationally cheap, making it a popular first choice in DMFT implementations. Within IPT, we calculate the self-energy only to second order. The first two terms in the perturbative expansion in terms of U are

1. The Hartree term, $\Sigma_\sigma = Un_{\bar{\sigma}}$, i.e., just a shift in the chemical potential *in the paramagnetic case.*
2. The Fock term arises from the exchange between two electrons of the same spin. Still, in the Hubbard model at hand, the interaction is an on-site interaction, and due to the exclusion principle, we only have interactions between electrons of opposite spins, thus the Fock term vanishes.

The second-order contribution to Σ is the skeleton diagram. This term captures the lowest-order dynamical correction to the self-energy beyond Hartree. It involves three bare Green's functions and is illustrated by the following expression:

$$\mathbf{\Sigma}(i\omega_n) = -\frac{U^2}{\beta^2}\sum_{\omega'_n,\Omega_m}\mathbf{G}^0(i\omega_n+i\Omega_m)\mathbf{G}^0(i\omega'_n+i\Omega_m)\mathbf{G}^0(i\omega'_n) \tag{138}$$

$\mathbf{G}^0$ is the bare propagator; in our case, it is the Weiss field of the AIM. $\omega_n^{(\prime)}$ and Ω_m are fermionic and bosonic Matsubara frequencies, respectively. In general, $\mathbf{\Sigma}$ and $\mathbf{G}$ are both matrices, but in the case of a single impurity orbital, they are just scalars. Using the spectral representation of $\mathbf{G}^0$

$$\mathbf{G}(i\omega_n) = \int d\omega \frac{\mathbf{A}(\omega)}{i\omega_n - \omega} \tag{139}$$

and the Fermi-Dirac distribution $f(\omega)$, we define:

$$A^+(\omega) = f(\omega)A(\omega) \tag{140}$$

$$A^-(\omega) = f(-\omega)A(\omega) \tag{141}$$

These represent the particle and hole parts of the spectral function. Performing analytic continuation $i\omega_n \to \nu + i\eta$, and taking the imaginary part, yields the expression for $\Im\Sigma(\nu)$:

$$\Im\Sigma(\nu) = -\pi U^2 \int d\omega d\omega' [A^-(\omega)A^+(\omega')A^-(\nu-\omega+\omega') + A^+(\omega)A^-(\omega')A^+(\nu-\omega+\omega')] \tag{142}$$

Furthermore, in our single-band model, which is particle-hole symmetric at half-filling, $A^+(\omega) = A^-(-\omega)$, and we have

$$\Im\Sigma(\nu) = -\pi U^2 \int d\omega' [A^+(\omega')[A^- * A^-](\nu+\omega') + A^-(\omega')[A^+ * A^+](\nu+\omega')] \tag{143}$$

$$= -\pi U^2([A^+ * [A^+ * A^+]](\nu) + [A^+ * [A^+ * A^+]](-\nu)) \tag{144}$$

Where the $*$ here means a convolution integral. We can get the real part using the Kramers-Kronig relations, since Σ is causal. For a more detailed derivation, see [23]. We will now employ this IPT solver in our DMFT loop to investigate the metal-insulator transition (MIT) in the half-filled Hubbard model. By scanning both increasing and decreasing interaction strength, we uncover hysteresis and phase coexistence, revealing the first-order nature of the transition and the underlying Mott physics.

6.3.1 Model and lattice choice.

We investigate the single–band Hubbard model at half-filling in the limit of infinite spatial dimensions ($d \to \infty$) or, equivalently, infinite lattice coordination $z \to \infty$.[1] In this limit the single-site dynamical mean-field theory (DMFT) is *exact*, because all non-local components of the self-energy vanish as $1/\sqrt{z}$. For concreteness we adopt the *Bethe lattice*, whose non-interacting density of states is the semicircle

$$D_0(\varepsilon) = \frac{2}{\pi D}\sqrt{1 - \left(\tfrac{\varepsilon}{D}\right)^2}, \qquad D = 2t^*,$$

with $t^* = t/\sqrt{z}$ the hopping rescaled so that D remains finite as $z \to \infty$. On the Bethe lattice the DMFT self-consistency integral (eq. 125) can be calculated explicitely, reducing the self-consistency condition to the simple form :

$$\mathcal{G}_0^{-1}(\omega) = \omega + \mu - {t^*}^2 G_{\mathrm{loc}}(\omega).$$

This provides an analytically transparent yet fully non-trivial framework to track the Mott metal–insulator transition (MIT).

Although no real crystal has $z = \infty$, the Bethe-lattice approximation captures the essential physics of three-dimensional compounds with *large but finite* coordination. A notable example is the corundum-structured oxide V_2O_3, whose sixfold connectivity yields a broad, nearly semicircular bandwidth; DMFT studies routinely model V_2O_3 with the Bethe-lattice density of states and obtain a quantitatively reasonable description of its pressure-driven Mott transition. See Fig. 18a.

6.3.2 Extreme Limits

We first investigate two extreme limits and compare them to our earlier approximate solutions: the non-interacting limit ($U = 0$) and the Insulating (High U) limit, shown in Fig. 13a and Fig. 13b, respectively. In the $U = 0$ case (Fig. 13a), one observes a single band crossing the Fermi level with no gap — the hallmark of a metallic, non-interacting system. In the High U case (Fig. 13b), the spectral function collapses into two well-separated Hubbard bands, characteristic of a Mott insulator. To illustrate the atomic limit explicitly, we ran a single iteration of the DMFT loop using second-order perturbation theory as the impurity solver. As expected, we find — apart from numerical broadening — two sharp peaks centered at $\pm U/2$, consistent with the spectral function of the single-site problem (see Fig. 7).

6.3.3 Quantum Phase Transition

Now that we have investigated the low- and high-U limits and confirmed agreement with our approximate methods, what about the region in between? We fix $T = 0.01t$ and vary the interaction strength U. In Fig. 14, we observe spectral weight transferring from the central quasiparticle peak at $\omega = 0$ toward the Hubbard bands. This signals an interaction-driven quantum phase transition. Near the critical U, the quasiparticle peak becomes extremely narrow and sharp — a hallmark of a heavy Fermi liquid — as shown in Fig. 14 (d).

[1] For a pedagogical review see G. Kotliar *et al.*, *Rev. Mod. Phys.* **68**, 13 (1996).

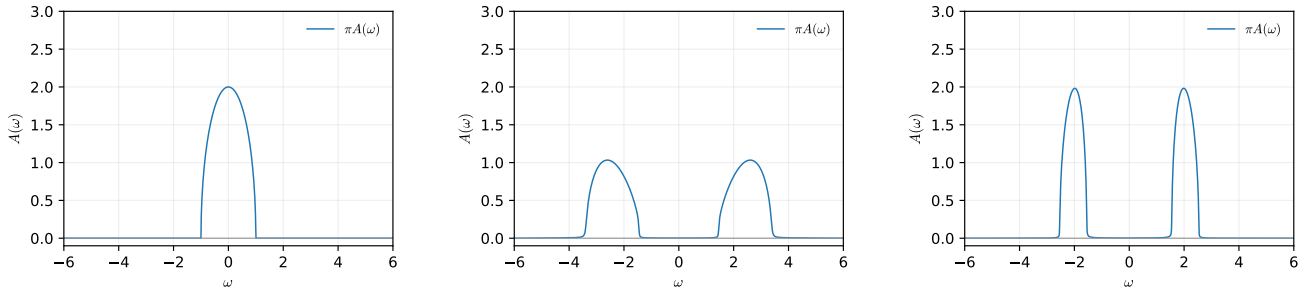

(a) Metallic Phase ($U = 0$): a single band at the Fermi level.

(b) Insulating limit ($t = 0$): two well-separated Hubbard bands indicating a Mott insulating state.

(c) Single iteration of DMFT at $U = 4$: spectral function of the single-site impurity showing two sharp peaks at $\pm U/2$.

Figure 13: Spectral functions in different limiting cases illustrating the transition from a non-interacting metal to a Mott insulator.

These cases highlight the core features of DMFT. At $U = 0$ (Fig. 14 (a), the system behaves as a non-interacting metal with a wide quasiparticle band crossing the Fermi level.

At intermediate coupling (Fig. 14 (c)), DMFT predicts a characteristic **three-peak structure**: a coherent quasiparticle peak (whose weight is Z) at $\omega = 0$, flanked by two incoherent Hubbard bands. As U increases, the weight of the quasiparticle peak diminishes, eventually vanishing at strong $U = 4t$, where a Mott insulator displays a wide gap setting between the Hubbard bands.

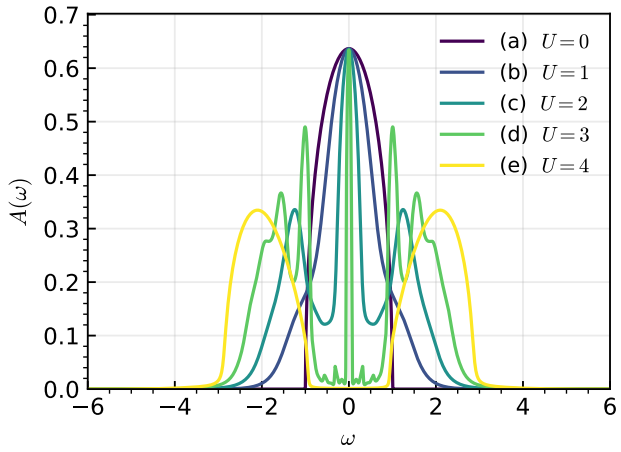

Figure 14: Evolution of the spectral function $\pi A(\omega)$ with increasing interaction strength U at fixed temperature $T = 0.01t$. (a) $U = 0.0$: A non-interacting metal with a single quasiparticle band crossing the Fermi level. (b) $U = 1.0$: The central quasiparticle peak narrows and Hubbard sidebands begin to emerge. (c) $U = 2.0$: A clear three-peak structure appears, with a coherent peak at $\omega = 0$ flanked by two incoherent Hubbard bands. (d) $U = 3.0$: The quasiparticle peak sharpens further, indicating heavy Fermi liquid behavior. (e) $U = 4.0$: The quasiparticle peak disappears, and only the Hubbard bands remain — a hallmark of the insulating regime.

6.3.4 Fermi Liquid Criterion

In the weakly correlated (metallic) regime the DMFT self-energy shows the characteristic Landau–Fermi-liquid behavior near $\omega = 0$. As seen in Fig. 15, the real part of $\Sigma(\omega)$ is linear in ω and the imaginary part scales as ω^2 for small ω, consistent with Landau theory. In particular $\Im\Sigma(0) = 0$, so quasiparticles have infinite lifetime at the Fermi level, and the quasiparticle weight $Z = [1 - \partial_\omega \Re\Sigma|_{\omega=0}]^{-1}$ is finite.

Increasing U makes the slope of $\Re\Sigma(\omega)$ steeper (smaller Z), but the low-ω FL scaling remains. In contrast, once the system becomes insulating, the self-energy develops a pole at $\omega = 0$. In that case, $\Re\Sigma$ diverges and $\Im\Sigma$ is large at low frequencies, cutting off the quasiparticle peak and opening a Mott gap (so that the density of states vanishes at $\omega = 0$). Thus, the shape of $\Sigma(\omega)$ in Fig. 15 unambiguously distinguishes the Fermi-liquid metal ($\Re\Sigma \propto \omega$, $\Im\Sigma \propto \omega^2$) from the Mott insulator (divergent self-energy).

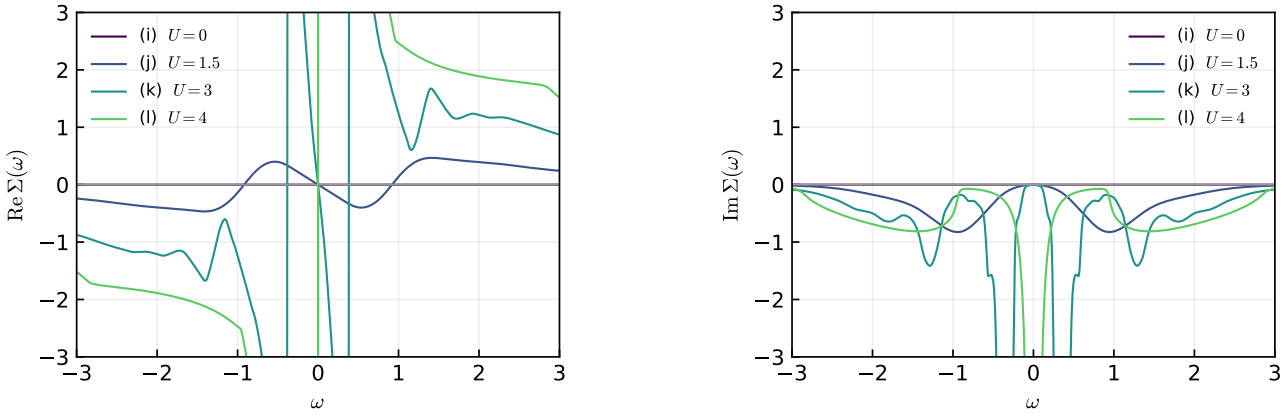

(a) Real part $\mathrm{Re}\,\Sigma(\omega)$.

(b) Imaginary part $\mathrm{Im}\,\Sigma(\omega)$.

Figure 15: DMFT self-energy near the Fermi level ($\omega \in [-3, 3]$) at $T = 0.01t$ for four interaction strengths: (i) $U = 0$, (j) $U = 1.5$, (k) $U = 3.0$, (l) $U = 4.0$. For $U \leq 1.5$ the system is a Fermi liquid: $\mathrm{Re}\,\Sigma(\omega) \propto \omega$ and $\mathrm{Im}\,\Sigma(\omega) \propto \omega^2$, giving finite quasiparticle weight Z. At $U = 3.0$ the slope of $\mathrm{Re}\,\Sigma$ steepens and $\mathrm{Im}\,\Sigma$ grows, indicating proximity to the Mott transition. At $U = 4.0$ a pole develops at $\omega = 0$: $\mathrm{Re}\,\Sigma$ diverges and $\mathrm{Im}\,\Sigma$ is large, signalling the insulating state where quasiparticles are suppressed.

6.3.5 Order Parameters

In this section, we study both the metal-to-insulator (MIT) and insulator-to-metal (IMT) transitions by identifying suitable order parameters and extracting the critical interaction strength U_c for each direction. We fix the temperature at $T = 0.01t$ and vary U across the transition. Typically, the metallic phase is characterized by the quasiparticle weight Z or the area under the coherent peak at $\omega = 0$, while the insulating phase is marked by the opening of a well-defined spectral gap. However, in our case, the analytic continuation introduces a finite broadening parameter η, which smears out the spectral features and effectively mimics finite temperature. This complicates the identification of a clear spectral gap and makes Z ill-defined near the transition point.

To overcome these challenges, we instead use the curvature of the spectral function at $\omega = 0$ as a unified quantity to characterize both phases. This curvature tracks the disappearance of the coherent peak in the metallic phase and its replacement by a dip in the insulating phase. Using this criterion, and aided by detailed plots of the spectral function near the transition, we estimate the critical values U_{c1} and U_{c2}. Our results confirm the existence of a coexistence region: both metallic and insulating solutions are locally stable, and the system converges to one or the other depending on the initial conditions and numerical details. See Fig. 16.

6.3.6 DMFT Phase Diagram and Comparison with Experiment: The Case of V_2O_3

The DMFT results on the infinite-coordination Bethe lattice yield the standard Mott phase diagram in the (U, T) plane. Figure 17 displays a metallic phase, an insulating phase, and the characteristic coexistence "dome": for $0 < T < T_c$, two solutions coexist within the window $U_{c1}(T) < U < U_{c2}(T)$. This dome terminates at a critical endpoint (U_c, T_c). Consider now a **fixed-U cut**, for instance at $U = 2.9$ (see vertical black arrow in Fig. 17, within the coexistence region). Increasing T along this path drives a first-order transition from the metallic to the insulating solution. Although these results are obtained in the infinite-dimensional Bethe lattice—an idealized limit—they closely mirror real experimental findings.

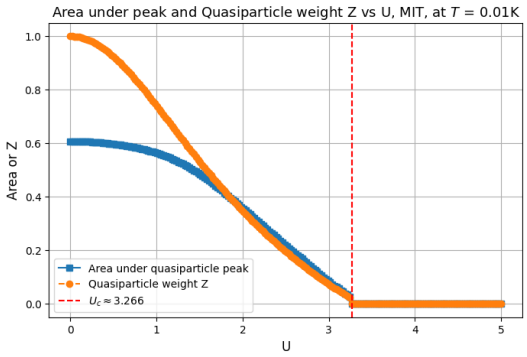

(a) MIT: Quasiparticle weight Z and area under the coherent peak vanish sharply at the critical $U_{c2} \approx 3.266$.

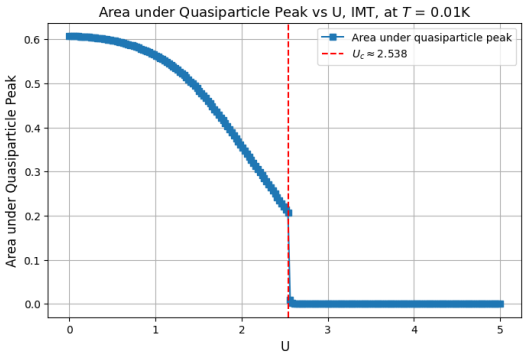

(b) IMT: The quasiparticle peak area grows continuously as U decreases, vanishing abruptly at $U_{c1} \approx 2.538$.

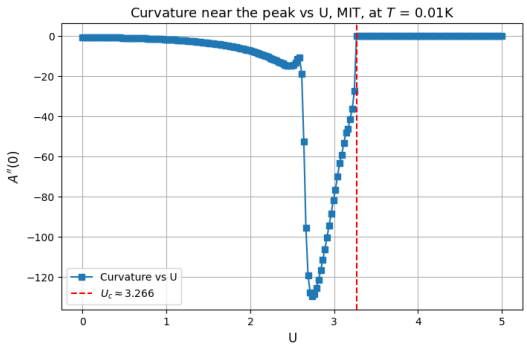

(c) MIT: Curvature of the spectral function at $\omega = 0$ drops and changes sign at the transition point.

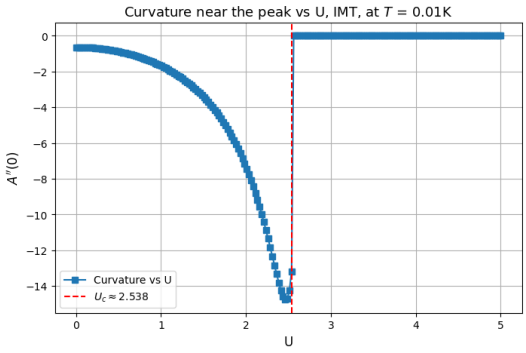

(d) IMT: Curvature also tracks the disappearance of the quasiparticle peak during the transition.

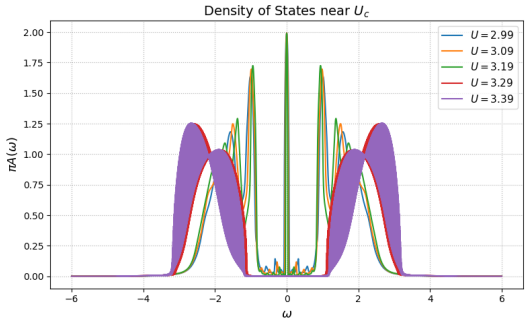

(e) DOS near U_{c2}: At low U, the central peak dominates; as $U \to U_c$, spectral weight shifts to the Hubbard bands.

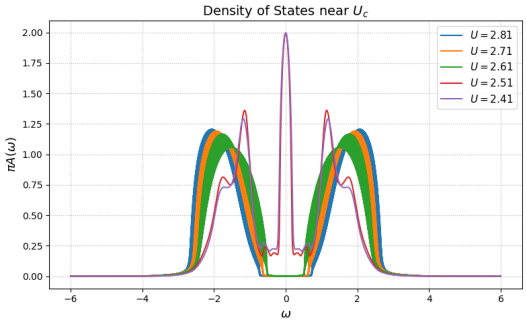

(f) DOS near U_{c1}: Hubbard bands collapse as $U \to U_c$, giving way to a central coherent peak.

Figure 16: Various order parameters and spectral features across the metal-insulator (MIT) and insulator-metal (IMT) transitions, computed at $T = 0.01t$. A sharp change is observed in the quasiparticle features, and the critical points for both directions are determined.

In particular, the canonical Mott system V_2O_3 displays remarkably similar behavior. As seen in Fig. 18a of ref. [24], Cr-doped V_2O_3 undergoes a first-order transition from a paramagnetic metal (PM) to a paramagnetic insulator (PI), with a critical endpoint—exactly the topology predicted by DMFT. This temperature-driven transition is clearly illustrated in Fig. 18b: at low T, the spectrum exhibits a sharp quasiparticle peak at the Fermi level. As T increases beyond a threshold, the peak abruptly vanishes, leaving only broad Hubbard sidebands and a gap at $\omega = 0$. This transition from a coherent Fermi liquid to a gapped Mott insulator reflects a thermally-induced metal $\to$ insulator transition—counter to the intuition that heating tends to increase conductivity.

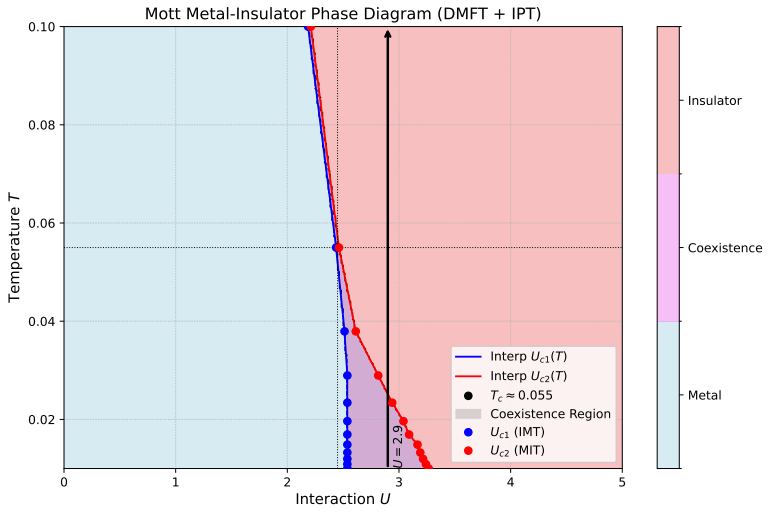

Figure 17: Phase diagram from DMFT on the Bethe lattice. The coexistence region, shaded in light gray, contains both metallic and insulating solutions. The dome ends at a critical point (U_c, T_c), beyond which the transition becomes continuous. A vertical cut at fixed $U = 2.9$ is shown as a black arrow.

We emphasize that our single-band DMFT neglects long-range magnetic ordering and thus only captures the *paramagnetic* Mott transition. In real V_2O_3, the low-T insulating phase is antiferromagnetic. However, the high-T PM-to-PI transition is well described within the DMFT framework.

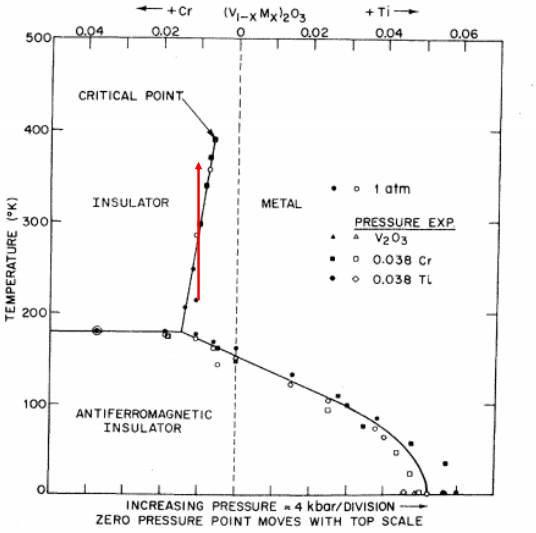

(a) Experimental phase diagram of Cr-doped V_2O_3 adapted from McWhan et al. [24], showing a first-order transition between paramagnetic metal and insulator, with a critical endpoint.

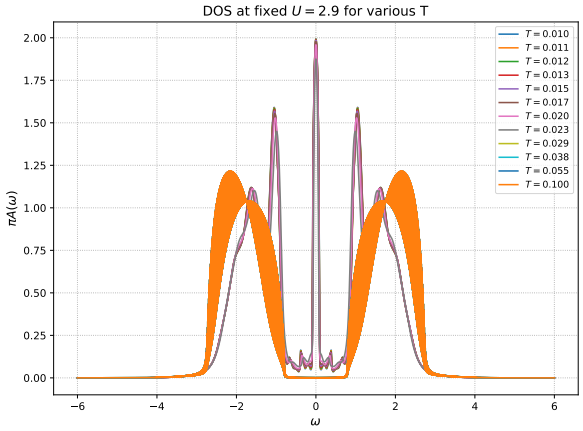

(b) Spectral evolution along a fixed-U cut at $U = 2.9$ across the coexistence region. Increasing T drives a first-order transition from metal to insulator.

Figure 18: Comparison between DMFT predictions and experimental observations in V_2O_3.

7 Conclusion

In this thesis, we investigated the metal-insulator transition in cuprates from both analytical and numerical perspectives, aiming to bridge the weak- and strong-coupling regimes within the Hubbard model framework. We began by discussing the physical context of high-T_c cuprates—strongly correlated materials whose parent compounds are Mott insulators. We then introduced the single-band Hubbard model as a minimal theoretical description, highlighting the competition between kinetic energy and local Coulomb repulsion.

Using analytical methods, we explored two limits of the Hubbard model. In the weak-coupling regime, a mean-field decoupling revealed an interaction-induced Slater gap driven by Fermi surface nesting and antiferromagnetic order. In the strong-coupling regime, a perturbative expansion in t/U yielded an effective Heisenberg model, with emergent spin exchange interactions scaling as $J = 4t^2/U$. These limits helped clarify the transition from a band insulator to a Mott insulator with localized magnetic moments.

To access the intermediate coupling regime, we employed Dynamical Mean-Field Theory (DMFT), a non-perturbative approach that treats local quantum fluctuations exactly. Using the IPT impurity solver, we computed the evolution of the spectral function and identified the characteristic three-peak structure in the metallic phase, with spectral weight transfer toward Hubbard bands as U increases. We captured the interaction-driven Mott transition and its first-order nature, along with a coexistence region and hysteresis.

Analyzing the self-energy and spectral curvature, we extracted critical interaction values and constructed a phase diagram that qualitatively reproduces the experimental phenomenology of canonical Mott systems such as V_2O_3. Although our single-band model neglects long-range magnetic order, it correctly captures the high-temperature paramagnetic Mott transition observed in experiments.

In summary, our study illustrates how the Hubbard model, coupled with DMFT, provides a unified framework for describing itinerant and localized phases in correlated electron systems. This work offers a solid foundation for future extensions to doped systems, cluster DMFT, or multiorbital settings more directly relevant to real materials.

A Weak-Coupling Mean-Field Theory

A standard first approximation to the full Hubbard Hamiltonian is to treat one term as a perturbation around the solvable limit of the other. Here, we begin from the non-interacting limit H_0, assuming that $U < t$ but still sufficiently strong to qualitatively modify the properties of the free Fermi gas. We apply a mean-field approximation to capture the effects of interactions. We rewrite the Hubbard Hamiltonian as $H = H_0 + H_1$, where

$$H_0 = \sum_{\mathbf{k},\sigma} \xi_{\mathbf{k}} c^\dagger_{\mathbf{k},\sigma} c_{\mathbf{k},\sigma} \tag{145}$$

$$H_1 = U \sum_j (n_{j\uparrow} - \frac{1}{2})(n_{j\downarrow} - \frac{1}{2}) = \sum_j \{U n_{j\uparrow} n_{j\downarrow} - \frac{U}{2}(n_{j\uparrow} + n_{j\downarrow})\} + \frac{U}{2} N \tag{146}$$

The last term is an overall shift in energy; we ignore it, and we redefine μ as $\tilde{\mu} := \mu + \frac{U}{2}$, which goes into $\xi_{\mathbf{k}}$ as $\tilde{\xi}_{\mathbf{k}} = \epsilon_{\mathbf{k}} - \tilde{\mu}$. We assume that fluctuations in the local occupation number $\langle n_{j,\sigma} \rangle$ are small, allowing us to linearize the interaction term around its mean value. We then introduce deviation operators as follows

$$\delta_{j,\uparrow} = n_{j,\uparrow} - \langle n_{j,\uparrow} \rangle \tag{147}$$

$$\delta_{j,\downarrow} = n_{j,\downarrow} - \langle n_{j,\downarrow} \rangle \tag{148}$$

We thus have

$$\begin{aligned} n_{j,\uparrow} n_{j,\downarrow} = (\langle n_{j,\uparrow} \rangle + \delta_{j,\uparrow})(\langle n_{j,\downarrow} \rangle + \delta_{j,\downarrow}) &= \langle n_{j,\uparrow} \rangle \langle n_{j,\downarrow} \rangle + \delta_{j,\uparrow} \langle n_{j,\downarrow} \rangle + \delta_{j,\downarrow} \langle n_{j,\uparrow} \rangle + \delta_{j,\uparrow} \delta_{j,\downarrow} \\ &\approx \langle n_{j,\uparrow} \rangle \langle n_{j,\downarrow} \rangle + \delta_{j,\uparrow} \langle n_{j,\downarrow} \rangle + \delta_{j,\downarrow} \langle n_{j,\uparrow} \rangle \\ &\approx \langle n_{j,\uparrow} \rangle \langle n_{j,\downarrow} \rangle + n_{j,\uparrow} \langle n_{j,\downarrow} \rangle + n_{j,\downarrow} \langle n_{j,\uparrow} \rangle \end{aligned} \tag{149}$$

Omitting the $\langle n_{j,\uparrow} \rangle \langle n_{j,\downarrow} \rangle$ term along with other terms, as they only add an energy shift. Finally, the Mean-Field HH is

$$H_{MF} = \sum_{\mathbf{k},\sigma} \tilde{\xi}_{\mathbf{k}} c^\dagger_{\mathbf{k},\sigma} c_{\mathbf{k},\sigma} + U \sum_j (n_{j,\uparrow} \langle n_{j,\downarrow} \rangle + n_{j,\downarrow} \langle n_{j,\uparrow} \rangle) \tag{150}$$

In half-filled materials ($\rho = 1$), antiferromagnetic (AFM) order is experimentally observed. To capture this, we introduce a staggered magnetization m_j defined as

$$m_j = \frac{1}{2}[\langle n_{j,\uparrow} \rangle - \langle n_{j,\downarrow} \rangle](-1)^{r+s} = m(-1)^{r+s} \tag{151}$$

where m is the sublattice magnetization density, the amplitude of the staggered spin pattern, and $\mathbf{R_j} = a(r, s)$. This definition is equivalent to assuming a magnetic order with a wave vector $\mathbf{q} = (\pi, \pi)/a$, corresponding to the nesting vector we have met before, which means that the magnetic pattern varies in space with periodicity described by $\mathbf{q}$, since

$$S^z_j = m(-1)^{r+s} = m e^{i\mathbf{q}\cdot\mathbf{R_j}} = m e^{i\pi(r+s)} \tag{152}$$

and $e^{i\mathbf{q}\cdot\mathbf{R_j}} = \pm 1$ depending on the sub-lattice $\mathbf{R_j}$ belongs to. We parameterize $\langle n_{j,\uparrow} \rangle$ and $\langle n_{j,\downarrow} \rangle$ in terms of m, as

$$\langle n_{j,\uparrow} \rangle = \frac{1}{2} + (-1)^{r+s} m \tag{153}$$

$$\langle n_{j,\downarrow} \rangle = \frac{1}{2} - (-1)^{r+s} m \tag{154}$$

When $m = 0$, $\langle n_{j,\uparrow} \rangle = \langle n_{j,\downarrow} \rangle = \frac{1}{2}$, and the system is paramagnetic. Whereas in the other extreme, we have $\langle n_j \rangle = \langle n_{j,\uparrow} \rangle = 1$ for, say, $r + s$ is even, and $\langle n_j \rangle = \langle n_{j,\downarrow} \rangle = -1$ for $r + s$ is odd, and we get a perfect AFM order. Focusing on a single sublattice, the AFM order effectively doubles the unit cell and leads to a $\pi/4$ rotation of the reciprocal lattice relative to the original square lattice. The old, primitive, and reciprocal lattice vectors were

$$\mathbf{a_1} = a(1, 0),\ \mathbf{a_2} = a(0, 1) \tag{155}$$

$$\mathbf{b_1} = \frac{2\pi}{a}(1, 0),\ \mathbf{b_2} = \frac{2\pi}{a}(0, 1) \tag{156}$$

In the new, $\frac{\pi}{4}$ rotated square, lattice, we have

$$\mathbf{a_1'} = a(1,-1),\ \mathbf{a_2'} = a(1,1) \tag{157}$$

$$\mathbf{b_1'} = \frac{\pi}{a}(1,-1),\ \mathbf{b_2'} = \frac{\pi}{a}(1,1) = \mathbf{q} \tag{158}$$

This means that the new Brillouin Zone F is half the size of the old one. Substituting into H_{MF}, we get

$$H_{MF}^{AF} = \sum_{\mathbf{k},\sigma} \tilde{\xi}_{\mathbf{k}} c_{\mathbf{k},\sigma}^{\dagger} c_{\mathbf{k},\sigma} + \sum_{j,\sigma} \frac{U}{2}[1 - 2m\sigma(-1)^{r+s}] c_{j,\sigma}^{\dagger} c_{j,\sigma} \tag{159}$$

$$H_{MF}^{AF} = \sum_{\mathbf{k},\sigma} \tilde{\xi}_{\mathbf{k}} c_{\mathbf{k},\sigma}^{\dagger} c_{\mathbf{k},\sigma} - mU \sum_{j,\sigma} \sigma(-1)^{r+s} c_{j,\sigma}^{\dagger} c_{j,\sigma} + \frac{U}{2} \sum_{j} n_j \tag{160}$$

The last term cancels the existing $\frac{U}{2}$ shift in the chemical potential, now reads $\tilde{\mu} = \mu$, and $\tilde{\xi}_{\mathbf{k}} = \xi_{\mathbf{k}}$. H_{MF}^{AF} now reads

$$H_{MF}^{AF} = \sum_{\mathbf{k},\sigma} \xi_{\mathbf{k}} c_{\mathbf{k},\sigma}^{\dagger} c_{\mathbf{k},\sigma} - mU \sum_{j,\sigma} \sigma e^{i\mathbf{q}\cdot\mathbf{R_j}} c_{j,\sigma}^{\dagger} c_{j,\sigma} \tag{161}$$

Using the definitions in equations (52) and (54), with $\mathbf{k} \in 1^{st}$ BZ, we see that the effect of $e^{i\mathbf{q}\cdot\mathbf{R_j}}$ is nesting the $\mathbf{k}$ vectors, and

$$H_{MF}^{AF} = \sum_{\mathbf{k},\sigma} \xi_{\mathbf{k}} c_{\mathbf{k},\sigma}^{\dagger} c_{\mathbf{k},\sigma} - mU \sum_{\mathbf{k},\sigma} \sigma c_{\mathbf{k}+\mathbf{q},\sigma}^{\dagger} c_{\mathbf{k},\sigma} \tag{162}$$

$$= \sum_{\mathbf{k},\sigma} \epsilon_{\mathbf{k}} c_{\mathbf{k},\sigma}^{\dagger} c_{\mathbf{k},\sigma} - \mu \sum_{\mathbf{k},\sigma} n_{\mathbf{k},\sigma} - mU \sum_{\mathbf{k},\sigma} \sigma c_{\mathbf{k}+\mathbf{q},\sigma}^{\dagger} c_{\mathbf{k},\sigma} \tag{163}$$

The effect of the third term is to scatter electrons from state $\mathbf{k}$ to $\mathbf{k}+\mathbf{q}$ without flipping the spin. We can easily verify the following properties

$$\epsilon_{\mathbf{k}+2\mathbf{q}} = \epsilon_{\mathbf{k}} \tag{164}$$

$$\epsilon_{\mathbf{k}+\mathbf{q}} = -\epsilon_{\mathbf{k}} \tag{165}$$

$$c_{\mathbf{k}+2\mathbf{q}} = c_{\mathbf{k}} \tag{166}$$

To diagonalize H_{MF}^{AF}, we use Heisenberg's equation of motion,

$$i\hbar \dot{c}_{\mathbf{k},\sigma} = [c_{\mathbf{k},\sigma}, H_{MF}^{AF}] \tag{167}$$

$$i\hbar \dot{c}_{\mathbf{k}+\mathbf{q},\sigma} = [c_{\mathbf{k}+\mathbf{q},\sigma}, H_{MF}^{AF}] \tag{168}$$

And noting that

$$[c_{\mathbf{k}',\sigma}, c_{\mathbf{k},\sigma}^{\dagger} c_{\mathbf{k},\sigma}] = \delta_{\mathbf{k}',\mathbf{k}} c_{\mathbf{k},\sigma} \tag{169}$$

$$[c_{\mathbf{k}',\sigma}, c_{\mathbf{k}+\mathbf{q},\sigma}^{\dagger} c_{\mathbf{k},\sigma}] = \delta_{\mathbf{k}',\mathbf{k}+\mathbf{q}} c_{\mathbf{k},\sigma} \tag{170}$$

we get,

$$i\hbar \dot{c}_{\mathbf{k},\sigma} = \xi_{\mathbf{k}} c_{\mathbf{k},\sigma} - \sigma mU c_{\mathbf{k}-\mathbf{q},\sigma} \tag{171}$$

$$i\hbar \dot{c}_{\mathbf{k}+\mathbf{q},\sigma} = \xi_{\mathbf{k}+\mathbf{q}} c_{\mathbf{k}+\mathbf{q},\sigma} - \sigma mU c_{\mathbf{k},\sigma} \tag{172}$$

by changing variables, $\mathbf{k} = \mathbf{k}+\mathbf{q}$, we get

$$i\hbar \dot{c}_{\mathbf{k},\sigma} = \xi_{\mathbf{k}} c_{\mathbf{k},\sigma} - \sigma mU c_{\mathbf{k}+\mathbf{q},\sigma} \tag{173}$$

$$i\hbar \dot{c}_{\mathbf{k}+\mathbf{q},\sigma} = \xi_{\mathbf{k}+\mathbf{q}} c_{\mathbf{k}+\mathbf{q},\sigma} - \sigma mU c_{\mathbf{k},\sigma} \tag{174}$$

which in the case of half-filling, $\mu = 0$, and we get

$$i\hbar\dot{c}_{\mathbf{k},\sigma} = \epsilon_{\mathbf{k}} c_{\mathbf{k},\sigma} - \sigma m U c_{\mathbf{k}+\mathbf{q},\sigma} \tag{175}$$

$$i\hbar\dot{c}_{\mathbf{k}+\mathbf{q},\sigma} = -\sigma m U c_{\mathbf{k},\sigma} - \epsilon_{\mathbf{k}} c_{\mathbf{k}+\mathbf{q},\sigma} \tag{176}$$

In a matrix form,

$$i\hbar \begin{pmatrix} \dot{c}_{\mathbf{k},\sigma} \\ \dot{c}_{\mathbf{k}+\mathbf{q},\sigma} \end{pmatrix} = \begin{pmatrix} \epsilon_{\mathbf{k}} & -\sigma\Delta \\ -\sigma\Delta & -\epsilon_{\mathbf{k}} \end{pmatrix} \begin{pmatrix} c_{\mathbf{k},\sigma} \\ c_{\mathbf{k}+\mathbf{q},\sigma} \end{pmatrix} \tag{177}$$

where $\Delta := mU$, $\mathbf{M}$ is time-evolution matrix defined as

$$\mathbf{M} = \begin{pmatrix} \epsilon_{\mathbf{k}} & -\sigma\Delta \\ -\sigma\Delta & -\epsilon_{\mathbf{k}} \end{pmatrix} \tag{178}$$

and

$$\mathbf{c}_{\mathbf{k},\sigma} = \begin{pmatrix} c_{\mathbf{k},\sigma} \\ c_{\mathbf{k}+\mathbf{q},\sigma} \end{pmatrix} \tag{179}$$

We could have done this differently; we split the BZ in the Half-Filling Hamiltonian into the reduced one and the part outside as follows

$$H^{AF}_{MF,\mu=0} = \sum_{\mathbf{k}\in F,\sigma} \left\{ \epsilon_{\mathbf{k}} c^{\dagger}_{\mathbf{k},\sigma} c_{\mathbf{k},\sigma} + \epsilon_{\mathbf{k}+\mathbf{q}} c^{\dagger}_{\mathbf{k}+\mathbf{q}\sigma} c_{\mathbf{k}+\mathbf{q}\sigma} - mU\sigma c^{\dagger}_{\mathbf{k}+\mathbf{q},\sigma} c_{\mathbf{k},\sigma} - mU\sigma c^{\dagger}_{\mathbf{k}+2\mathbf{q},\sigma} c_{\mathbf{k}+\mathbf{q},\sigma} \right\} \tag{180}$$

$$= \sum_{\mathbf{k}\in F,\sigma} \begin{pmatrix} c^{\dagger}_{\mathbf{k},\sigma} & c^{\dagger}_{\mathbf{k}+\mathbf{q},\sigma} \end{pmatrix} \begin{pmatrix} \epsilon_{\mathbf{k}} & -\sigma\Delta \\ -\sigma\Delta & -\epsilon_{\mathbf{k}} \end{pmatrix} \begin{pmatrix} c_{\mathbf{k},\sigma} \\ c_{\mathbf{k}+\mathbf{q},\sigma} \end{pmatrix} \tag{181}$$

$$= \sum_{\mathbf{k}\in F,\sigma} \mathbf{c}^{\dagger}_{\mathbf{k},\sigma} \mathbf{M} \mathbf{c}_{\mathbf{k},\sigma} \tag{182}$$

In either case, the matrix that needs to be diagonalised is the same $\mathbf{M}$. To do so, we need a unitary matrix $\mathbf{S}$ such that

$$i\hbar\dot{c}_{\mathbf{k},\sigma} = \mathbf{M}\mathbf{c}_{\mathbf{k},\sigma} \tag{183}$$

$$i\hbar\mathbf{S}^{-1}\dot{c}_{\mathbf{k},\sigma} = \mathbf{S}^{-1}\mathbf{M}\mathbf{S}\mathbf{S}^{-1}\mathbf{c}_{\mathbf{k},\sigma} \tag{184}$$

$$i\hbar\dot{d}_{\mathbf{k},\sigma} = \mathbf{D}\mathbf{d}_{\mathbf{k},\sigma} \tag{185}$$

where $\mathbf{D}$ is the diagonal matrix written in terms of the eigenvalues of $\mathbf{M}$ as

$$\mathbf{d}_{\mathbf{k},\sigma} = \mathbf{S}^{-1}\mathbf{c}_{\mathbf{k},\sigma} \tag{186}$$

$$\mathbf{D} = \begin{pmatrix} E^1_{\mathbf{k}} & 0 \\ 0 & E^2_{\mathbf{k}} \end{pmatrix} \tag{187}$$

and, $E^{1(2)}_{\mathbf{k}} = \pm\sqrt{\epsilon^2_{\mathbf{k}} + \Delta^2} = \pm E_{\mathbf{k}}$. Finally, $\mathbf{S}$ is built from the eigenvectors of $\mathbf{M}$, and it is give by

$$\mathbf{S} = \begin{pmatrix} \sigma u_{\mathbf{k}} & -v_{\mathbf{k}} \\ v_{\mathbf{k}} & \sigma u_{\mathbf{k}} \end{pmatrix} \tag{188}$$

and $u_{\mathbf{k}}, v_{\mathbf{k}}$ are defined as

$$u_{\mathbf{k}} = \frac{\gamma_{\mathbf{k}}}{\sqrt{1+\gamma^2_{\mathbf{k}}}},\ v_{\mathbf{k}} = \frac{1}{\sqrt{1+\gamma^2_{\mathbf{k}}}} \tag{189}$$

$$\gamma_{\mathbf{k}} := \frac{\Delta}{\epsilon_{\mathbf{k}} - E_{\mathbf{k}}},\ \beta_{\mathbf{k}} := \frac{\epsilon_{\mathbf{k}} + E_{\mathbf{k}}}{\Delta} \tag{190}$$

with the condition

$$\sigma\gamma_{\mathbf{k}} = -\frac{1}{\sigma}\beta_{\mathbf{k}} \tag{191}$$

In terms of $\mathbf{D}$, $H^{AF}_{MF,\mu=0}$ is now

$$H^{AF}_{MF,\mu=0} = \sum_{\mathbf{k}\in BZ,\sigma} E_{\mathbf{k}}\{d^{\dagger}_{\mathbf{k},\sigma}d_{\mathbf{k},\sigma} - d^{\dagger}_{\mathbf{k}+\mathbf{q}\sigma}d_{\mathbf{k}+\mathbf{q}\sigma}\} \tag{192}$$

There is still one last step, to insure that $\mathbf{S}$ is indeed unitary, i.e. conserves the anti-commutation relations, assuming that $u_{\mathbf{k}}$ and $v_{\mathbf{k}}$ are real,

$$\begin{aligned}
\delta_{\mathbf{k},\mathbf{k}'} = \{c_{\mathbf{k},\sigma}, c^{\dagger}_{\mathbf{k}',\sigma}\} &= \{\sigma u_{\mathbf{k}}d_{\mathbf{k},\sigma} + v_{\mathbf{k}}d_{\mathbf{k}+\mathbf{q},\sigma}, \sigma u_{\mathbf{k}'}d^{\dagger}_{\mathbf{k}',\sigma} + v_{\mathbf{k}'}d^{\dagger}_{\mathbf{k}'+\mathbf{q},\sigma}\} \\
&= \sigma^2 u_{\mathbf{k}}u_{\mathbf{k}'}\{d_{\mathbf{k},\sigma}, d^{\dagger}_{\mathbf{k}',\sigma}\} + v_{\mathbf{k}}v_{\mathbf{k}'}\{d_{\mathbf{k}+\mathbf{q},\sigma}, d^{\dagger}_{\mathbf{k}'+\mathbf{q},\sigma}\} \qquad (193)\\
&- \sigma u_{\mathbf{k}}v_{\mathbf{k}'}\{d_{\mathbf{k},\sigma}, d^{\dagger}_{\mathbf{k}'+\mathbf{q},\sigma}\} - \sigma v_{\mathbf{k}}u_{\mathbf{k}'}\{d_{\mathbf{k}+\mathbf{q},\sigma}, d^{\dagger}_{\mathbf{k}',\sigma}\} \\
&= \sigma^2 u_{\mathbf{k}}u_{\mathbf{k}'}\delta_{\mathbf{k},\mathbf{k}'} + v_{\mathbf{k}}v_{\mathbf{k}'}\delta_{\mathbf{k}+\mathbf{q},\mathbf{k}'+\mathbf{q}} - \sigma u_{\mathbf{k}}v_{\mathbf{k}'}\delta_{\mathbf{k},\mathbf{k}'+\mathbf{q}} - \sigma v_{\mathbf{k}}u_{\mathbf{k}'}\delta_{\mathbf{k}+\mathbf{q},\mathbf{k}'} \\
&= (u^2_{\mathbf{k}} + v^2_{\mathbf{k}})\delta_{\mathbf{k},\mathbf{k}'} - \sigma u_{\mathbf{k}}v_{\mathbf{k}'}\delta_{\mathbf{k},\mathbf{k}'} - \sigma v_{\mathbf{k}}u_{\mathbf{k}'}\delta_{\mathbf{k}+\mathbf{q},\mathbf{k}'} \qquad (194)
\end{aligned}$$

This equation is satisfied if

$$u^2_{\mathbf{k}} + v^2_{\mathbf{k}} = 1 \tag{195}$$

$$\delta_{\mathbf{k},\mathbf{k}'} = \delta_{\mathbf{k}+\mathbf{q},\mathbf{k}'} = 0 \tag{196}$$

This is indeed the case if we restricted the sum over $\mathbf{k}$ to the reduced BZ, F, in that case, $\mathbf{k}, \mathbf{k}' + \mathbf{q}$ are never equal, same for $\mathbf{k} + \mathbf{q}, \mathbf{k}'$, and the final diagonalized Hamiltonian is now

$$H^{AF}_{MF,\mu=0} = \sum_{\mathbf{k}\in F,\sigma} E_{\mathbf{k}}\{d^{\dagger}_{\mathbf{k},\sigma}d_{\mathbf{k},\sigma} - d^{\dagger}_{\mathbf{k}+\mathbf{q}\sigma}d_{\mathbf{k}+\mathbf{q}\sigma}\} \tag{197}$$

The resulting model describes a two-band insulator with an energy gap of $2\Delta = 2mU$ at half-filling, capturing the insulating behavior observed in the parent compounds of cuprates.

We have assumed an AFM order with m magnetisation, now, we calculate m self-consistently. First, we calculate it from $H^{AF}_{MF,\mu=0}$ and then equate it to its assumed values in $m = \frac{1}{N}\sum_j \frac{(-1)^j}{2}[\langle n_{j,\uparrow}\rangle - \langle n_{j,\downarrow}\rangle]$.

$$n_{j,\sigma} = c^{\dagger}_{j,\sigma}c_{j,\sigma} = \frac{1}{N}\sum_{\mathbf{k},\mathbf{k}'} e^{-i(\mathbf{k}-\mathbf{k}').\mathbf{R_j}}c^{\dagger}_{\mathbf{k},\sigma}c_{\mathbf{k}',\sigma} \tag{198}$$

Recall that

$$\mathbf{c}_{\mathbf{k},\sigma} = \mathbf{S}\mathbf{d}_{\mathbf{k},\sigma} \tag{199}$$

$$\begin{pmatrix} c_{\mathbf{k},\sigma} \\ c_{\mathbf{k}+\mathbf{q},\sigma} \end{pmatrix} = \begin{pmatrix} \sigma u_{\mathbf{k}} & -v_{\mathbf{k}} \\ v_{\mathbf{k}} & \sigma u_{\mathbf{k}} \end{pmatrix} \begin{pmatrix} d_{\mathbf{k},\sigma} \\ d_{\mathbf{k}+\mathbf{q},\sigma} \end{pmatrix} \tag{200}$$

which gives

$$c_{\mathbf{k},\sigma} = \sigma u_{\mathbf{k}}d_{\mathbf{k},\sigma} - v_{\mathbf{k}}d_{\mathbf{k}+\mathbf{q},\sigma} \tag{201}$$

$$c^{\dagger}_{\mathbf{k},\sigma} = \sigma u_{\mathbf{k}}d^{\dagger}_{\mathbf{k},\sigma} - v_{\mathbf{k}}d^{\dagger}_{\mathbf{k}+\mathbf{q},\sigma} \tag{202}$$

$$c_{\mathbf{k}+\mathbf{q},\sigma} = v_{\mathbf{k}}d_{\mathbf{k},\sigma} + \sigma u_{\mathbf{k}}d_{\mathbf{k}+\mathbf{q},\sigma} \tag{203}$$

$$c^{\dagger}_{\mathbf{k}+\mathbf{q},\sigma} = v_{\mathbf{k}}d^{\dagger}_{\mathbf{k},\sigma} + \sigma u_{\mathbf{k}}d^{\dagger}_{\mathbf{k}+\mathbf{q},\sigma} \tag{204}$$

$$m = \frac{1}{N}\sum_j \frac{(-1)^j}{2}[\langle n_{j,\uparrow}\rangle - \langle n_{j,\downarrow}\rangle] = \frac{1}{2N}\sum_{\mathbf{k},\mathbf{k}'}\Big\{\frac{1}{N}\sum_j e^{-i(\mathbf{k}-\mathbf{k}'-\mathbf{q}).\mathbf{R_j}}\Big\}\langle c^{\dagger}_{\mathbf{k},\uparrow}c_{\mathbf{k}',\uparrow} - c^{\dagger}_{\mathbf{k},\downarrow}c_{\mathbf{k}',\downarrow}\rangle \tag{205}$$

$$= \frac{1}{2N}\sum_{\mathbf{k}}\langle c^{\dagger}_{\mathbf{k}+\mathbf{q},\uparrow}c_{\mathbf{k},\uparrow} - c^{\dagger}_{\mathbf{k}+\mathbf{q},\downarrow}c_{\mathbf{k},\downarrow}\rangle \tag{206}$$

Where we have used, $(-1)^j = e^{i\mathbf{q}.\mathbf{R_j}}$, with $\mathbf{q} = \frac{\pi}{a}(1,1)$, and $\left\{\frac{1}{N}\sum_j e^{-i(\mathbf{k}-\mathbf{k}'-\mathbf{q}).\mathbf{R_j}}\right\} = N\delta_{\mathbf{k},\mathbf{k}'+\mathbf{q}}$. Now, $\mathbf{k}$ in the sum runs over the full BZ, and the expressions of $c_{\mathbf{k},\sigma}c_{\mathbf{k}+\mathbf{q},\sigma}$ in terms of the d operators run over F, so we have to separate the sum into two terms to cover the same values of $\mathbf{k}$, but the sum now runs only over F as follows

$$m = \frac{1}{2N}\sum_{\mathbf{k}\in F}\langle c^\dagger_{\mathbf{k}+\mathbf{q},\uparrow}c_{\mathbf{k},\uparrow} + c^\dagger_{\mathbf{k}+2\mathbf{q},\uparrow}c_{\mathbf{k}+\mathbf{q},\uparrow} - c^\dagger_{\mathbf{k}+\mathbf{q},\downarrow}c_{\mathbf{k},\downarrow} - c^\dagger_{\mathbf{k}+2\mathbf{q},\downarrow}c_{\mathbf{k}+\mathbf{q},\downarrow}\rangle \tag{207}$$

Recalling that, $c_{\mathbf{k}+2\mathbf{q}} = c_{\mathbf{k}}$, we get

$$m = \frac{1}{2N}\sum_{\mathbf{k}\in F}\langle c^\dagger_{\mathbf{k}+\mathbf{q},\uparrow}c_{\mathbf{k},\uparrow} + c^\dagger_{\mathbf{k},\uparrow}c_{\mathbf{k}+\mathbf{q},\uparrow} - c^\dagger_{\mathbf{k}+\mathbf{q},\downarrow}c_{\mathbf{k},\downarrow} - c^\dagger_{\mathbf{k},\downarrow}c_{\mathbf{k}+\mathbf{q},\downarrow}\rangle \tag{208}$$

Using the expressions for the cs in terms of the diagonal operators, and recalling that at half-filling only the lower band is filled, namely the one associated with $d^\dagger_{\mathbf{k}+\mathbf{q},\sigma}$. This means that taking the expected value over the GS, the only nonzero term will be

$$\langle d^\dagger_{\mathbf{k}+\mathbf{q},\sigma}d_{\mathbf{k}+\mathbf{q},\sigma}\rangle = 1 \longrightarrow \langle c^\dagger_{\mathbf{k}+\mathbf{q},\sigma}c_{\mathbf{k},\sigma}\rangle = \langle c^\dagger_{\mathbf{k},\sigma}c_{\mathbf{k}+\mathbf{q},\sigma}\rangle = -\sigma u_{\mathbf{k}}v_{\mathbf{k}} \tag{209}$$

This leads to

$$m = \frac{1}{N}\sum_{\mathbf{k}\in F}\{-2u_{\mathbf{k}}v_{\mathbf{k}}\} \tag{210}$$

and using the definitions for $u_{\mathbf{k}}$ and $v_{\mathbf{k}}$, we get

$$u_{\mathbf{k}}v_{\mathbf{k}} = -\frac{\Delta}{2E_{\mathbf{k}}} \tag{211}$$

$$1 = \frac{U}{N}\sum_{\mathbf{k}\in F}\frac{1}{E_{\mathbf{k}}} \tag{212}$$

Going to the continuum limit, i.e. $N \to \infty$,

$$1 = U(\frac{a}{2\pi})^2\int_F \frac{dk^2}{\sqrt{\epsilon^2_{\mathbf{k}} + \Delta^2}} \tag{213}$$

Going to polar coordinates, changing variables from k to ϵ, where as $|\mathbf{k}|$ goes from $(0,0)$ to $(\frac{\pi}{2a}, \frac{\pi}{2a})$, $\epsilon \in (-4t, 0)$, and introducing the density of states $\rho(\epsilon)$, we get

$$1 = U\int_{-4t}^{0}\rho(\epsilon)\frac{d\epsilon}{\sqrt{\epsilon^2 + \Delta^2}} \tag{214}$$

changing variables again $\epsilon \longrightarrow -\epsilon$ with $\rho(-\epsilon) = \rho(\epsilon)$, recall that we have two bands symmetric around $\epsilon = 0$, we get

$$1 = U\int_{0}^{4t}\rho(\epsilon)\frac{d\epsilon}{\sqrt{\epsilon^2 + \Delta^2}} \tag{215}$$

In the weak-coupling limit ($U \ll t$) we assume a small but finite order parameter Δ. Because the two-dimensional density of states diverges logarithmically,

$$\rho(\epsilon) \;\approx\; \frac{1}{2\pi^2 t}\,\ln\frac{8t}{|\epsilon|},$$

the k-space integral that enters the mean-field gap equation is dominated by energies $|\epsilon| \lesssim \Delta$:

$$\frac{1}{U} \;=\; \int_{-W}^{W}\frac{\rho(\epsilon)\,d\epsilon}{2\sqrt{\epsilon^2+\Delta^2}} \;\simeq\; \frac{1}{2\pi^2 t}\,\ln\frac{16t}{\Delta},$$

where $W = 4t$ is the half-bandwidth. Solving for Δ yields

$$\boxed{\;\Delta \;=\; 16\,t\,\exp\!\Big[-2\pi\sqrt{\tfrac{t}{U}}\Big]\;}$$

(the numerical prefactor depends on the ultraviolet cut-off and is therefore non-universal).

As $U \to 0$ the gap collapses, but the square-root exponent makes the approach much slower than the usual $\exp(-\text{const}\, t/U)$ found in metals with a finite $\rho(0)$. Consequently, even weak interactions favour antiferromagnetic order on the square lattice. For the opposite situation, $U >> t$, and $\Delta >> t$ dominates the integrand denominator. Thus, we find approximately

$$1 = \frac{U}{\Delta} \int_0^{4t} \rho(\epsilon) d\epsilon \tag{216}$$

But since $\int_{-4t}^{4t} \rho(\epsilon) d\epsilon = 1$, then $\Delta = U/2$. As U increases further, Δ approaches U, consistent with the Mott gap identified in the single-site Hubbard model.

B Strong-Coupling Expansion

We look for an effective Hamiltonian that describes the physics in the lowest Hubbard subband, namely the one with no doubly occupied sites. We are treating the kinetic energy as a perturbation, so we first divide it into three parts depending on how the parts change the total number of doubly occupied sites, H^0, H^-, H^+. To do so, we introduce the projection operators on the four single-site states defined as

$$\hat{P}_{j0} = |0\rangle_j \langle 0| = (1-n_{j\uparrow})(1-n_{j\downarrow}) \tag{217}$$

$$\hat{P}_{j\sigma} = n_{j\sigma}(1-n_{j-\sigma}) \tag{218}$$

$$\hat{P}_{jd} = |d\rangle_j \langle d| = n_{j\uparrow}n_{j\downarrow} \tag{219}$$

$$\hat{P}_{j0} + \hat{P}_{j\uparrow} + \hat{P}_{j\downarrow} + \hat{P}_{jd} = \mathbb{I}$$

Using these operators, we can identify the different processes in H_1, for example, consider the case where site 2 has an $\uparrow$ electron and site 1 has an $\downarrow$ electron, the operator $c^\dagger_{1\uparrow}c_{2\uparrow}$ would increase the number of doubly occupied sites by one by transferring the $\uparrow$ electron from site 2 to site 1, and to single out this process we have the following term,

$$\hat{P}_{1d}c^\dagger_{1\uparrow}c_{2\uparrow}\hat{P}_{2\uparrow} \tag{220}$$

collecting all terms that increase the number of d sites, we get

$$H^+ = -t\sum_\sigma \Big\{ \hat{P}_{1d}c^\dagger_{1\sigma}c_{2\sigma}\hat{P}_{2\sigma} + \hat{P}_{2d}c^\dagger_{2\sigma}c_{1\sigma}\hat{P}_{1\sigma} \Big\} \tag{221}$$

Similarly, we have

$$H^- = -t\sum_\sigma \Big\{ \hat{P}_{1\sigma}c^\dagger_{1\sigma}c_{2\sigma}\hat{P}_{2d} + \hat{P}_{2\sigma}c^\dagger_{2\sigma}c_{1\sigma}\hat{P}_{1d} \Big\} \tag{222}$$

$$H^0 = -t\sum_\sigma \Big\{ \hat{P}_{1d}c^\dagger_{1\sigma}c_{2\sigma}\hat{P}_{2d} + \hat{P}_{2\sigma}c^\dagger_{2\sigma}c_{1\sigma}\hat{P}_{1\sigma} + H.C. \Big\} \tag{223}$$

Using the expression for the projection operators, and the following properties

$$n_{j\sigma}c^\dagger_{j\sigma} = c^\dagger_{j\sigma} \tag{224}$$

$$n_{j\sigma}c_{j\sigma} = 0 \tag{225}$$

$$c^\dagger_{j\sigma}n_{j\sigma} = 0 \tag{226}$$

$$c_{j\sigma}n_{j\sigma} = c_{j\sigma} \tag{227}$$

we get

$$\hat{P}_{1d}c^\dagger_{1\sigma}c_{2\sigma}\hat{P}_{2\sigma} = n_{1(-\sigma)}c^\dagger_{1\sigma}c_{2\sigma}(1-n_{2(-\sigma)}) \tag{228}$$

$$\hat{P}_{2d}c^\dagger_{2\sigma}c_{1\sigma}\hat{P}_{1\sigma} = n_{2(-\sigma)}c^\dagger_{2\sigma}c_{1\sigma}(1-n_{1(-\sigma)}) \tag{229}$$

$$\hat{P}_{1\sigma}c^\dagger_{1\sigma}c_{2\sigma}\hat{P}_{2d} = (1-n_{1(-\sigma)})c^\dagger_{1\sigma}c_{2\sigma}n_{2(-\sigma)} \tag{230}$$

$$\hat{P}_{2\sigma}c^\dagger_{2\sigma}c_{1\sigma}\hat{P}_{1d} = (1-n_{2(-\sigma)})c^\dagger_{2\sigma}c_{1\sigma}n_{1(-\sigma)} \tag{231}$$

$$\hat{P}_{1d}c^\dagger_{1\sigma}c_{2\sigma}\hat{P}_{2d} = n_{1(-\sigma)}c^\dagger_{1\sigma}c_{2\sigma}n_{2(-\sigma)} \tag{232}$$

$$\hat{P}_{2\sigma}c^\dagger_{2\sigma}c_{1\sigma}\hat{P}_{1\sigma} = (1-n_{2(-\sigma)})c^\dagger_{2\sigma}c_{1\sigma}(1-n_{1(-\sigma)})) \tag{233}$$

The total Hamiltonian is $H = H^0 + H^+ + H^- + H^U$. Our goal is to eliminate, at least to leading order in t, the transitions between the low-energy and high-energy Hubbard subbands. We use a kind of Schrieffer–Wolff unitary transformation S to go to a new basis where this is possible as follows

$$H_{eff} = e^{iS}He^{-iS} = H + i[S,H] + \frac{i^2}{2}[S,[S,H]] + ... \tag{234}$$

$$= H^0 + H^+ + H^- + H^U + i[S,H^U] + i[S,H^+ + H^-] + i[S,H^0] + \frac{i^2}{2}[S,[S,H]] + ... \tag{235}$$

We want to build S from H^+ and H^-, to get a hint, we commute one term in H^+ with H^U,we have

$$[n_{1\downarrow}c^\dagger_{1\uparrow}c_{2\uparrow}(1-n_{2\downarrow}), n_{1\uparrow}n_{1\downarrow}] = -n_{1\downarrow}c^\dagger_{1\uparrow}c_{2\uparrow}(1-n_{2\downarrow}) \tag{236}$$

and similarly

$$[H^+, H_U] = -UH^+ \tag{237}$$
$$[H^-, H_U] = UH^- \tag{238}$$

Thus, choosing S to be

$$S = -\frac{i}{U}(H^+ - H^-) \tag{239}$$

and then

$$i[S, H^U] = \frac{1}{U}[H^+ - H^-, H^U] = -(H^+ + H^-) \tag{240}$$
$$i[S, H^+ + H^-] = \frac{2}{U}[H^+, H^-], \text{ of the order of } \frac{t^2}{U} \tag{241}$$
$$\frac{i^2}{2}[S,[S,H^U]] = -\frac{1}{U}[H^+, H^-] \tag{242}$$

Note that we ignored the term

$$\frac{i^2}{2}[S,[S,H^+ + H^-]] = \frac{i}{U}[S,[H^+,H^-]] = \frac{1}{U^2}\left\{[H^+,[H^+,H^-]] - [H^-,[H^+,H^-]]\right\} \tag{243}$$

which is of order $O(\frac{t^3}{U^2})$, and we ignore any contributions coming from $i[S,H^0]$ and $\frac{i^2}{2}[S,[S,H^0]]$ justified below, and we sum the other terms to $O(t)$, we get

$$H_{eff} = H^0 + H^U + \frac{1}{U}[H^+, H^-] \tag{244}$$

Recall that we are considering the half-filling case where the lowest subband, in this two-site Hubbard Hamiltonian, contains one electron at each site. In this case, there are no double occupations, and of course, we cannot decrease them, thus there are no contributions from H^U and H^-, furthermore, there is no hopping that conserves the number of double occupied sites, i.e. no contributions from H^0, and we end up with

$$H_{eff} = -\frac{1}{U}H^-H^+ \tag{245}$$

To understand the meaning of our result, recall that in the half-filled two-site Hubbard model, the full Hilbert space is spanned by

$$|\uparrow,\uparrow\rangle, |\downarrow,\downarrow\rangle, |\uparrow,\downarrow\rangle, |\downarrow,\uparrow\rangle, |\uparrow\uparrow,0\rangle, |0,\uparrow\uparrow\rangle, |\downarrow\downarrow,0\rangle, |0,\downarrow\downarrow\rangle \tag{246}$$

Now that we have used a unitary transformation to go to a different basis in which the lowest Hubbard sub-band, $|\uparrow,\uparrow\rangle, |\downarrow,\downarrow\rangle, |\uparrow,\downarrow\rangle, |\downarrow,\uparrow\rangle$ doesn't couple to the higher ones, $|\uparrow\uparrow,0\rangle, |0,\uparrow\uparrow\rangle, |\downarrow\downarrow,0\rangle, |0,\downarrow\downarrow\rangle$, with the notation $|\text{site 1}, \text{site 2}\rangle$. In the original basis, H_{eff} describes virtual transitions into higher-energy doubly occupied states and back. In the transformed basis—restricted to the singly occupied subspace—these virtual processes manifest as effective spin exchange, i.e., spin fluctuations. To understand the effect of H_{eff}, we calculate the matrix elements of H_{eff} in the lowest sub-band, with the convention that

$$|\uparrow,\downarrow\rangle = c^\dagger_{1\uparrow}c^\dagger_{2\downarrow}|0,0\rangle \tag{247}$$
$$|\uparrow\downarrow,0\rangle = c^\dagger_{1\uparrow}c^\dagger_{1\downarrow}|0,0\rangle \tag{248}$$

we get

$$H_{eff}|\uparrow,\uparrow\rangle = H_{eff}|\downarrow,\downarrow\rangle = 0 \tag{249}$$
$$\langle\uparrow,\downarrow|H_{eff}|\uparrow,\downarrow\rangle = \langle\downarrow,\uparrow|H_{eff}|\downarrow,\uparrow\rangle = -2\frac{t^2}{U} \tag{250}$$
$$\langle\uparrow,\downarrow|H_{eff}|\downarrow,\uparrow\rangle = \langle\downarrow,\uparrow|H_{eff}|\uparrow,\downarrow\rangle = +2\frac{t^2}{U} \tag{251}$$

The factor of 2 arises because the electron can be removed from either site first—the two sequences are indistinguishable and therefore add coherently, and the difference of sign is because we have to pay attention to the convention used in defining the states. We present the calculations of one matrix element, namely $\langle\uparrow,\downarrow|H_{eff}|\uparrow,\downarrow\rangle$. First, H_{eff} is given by

$$H_{eff} = -\frac{t^2}{U}\sum_{\sigma,\sigma'}\Big\{\hat{P}_{1\sigma}c^\dagger_{1\sigma}c_{2\sigma}\hat{P}_{2d}\hat{P}_{1d}c^\dagger_{1\sigma'}c_{2\sigma'}\hat{P}_{2\sigma'} \tag{252}$$

$$+\hat{P}_{2\sigma}c^\dagger_{2\sigma}c_{1\sigma}\hat{P}_{1d}\hat{P}_{1d}c^\dagger_{1\sigma'}c_{2\sigma'}\hat{P}_{2\sigma'} \tag{253}$$

$$+\hat{P}_{1\sigma}c^\dagger_{1\sigma}c_{2\sigma}\hat{P}_{2d}\hat{P}_{2d}c^\dagger_{2\sigma'}c_{1\sigma'}\hat{P}_{1\sigma'} \tag{254}$$

$$+\hat{P}_{2\sigma}c^\dagger_{2\sigma}c_{1\sigma}\hat{P}_{1d}\hat{P}_{2d}c^\dagger_{2\sigma'}c_{1\sigma'}\hat{P}_{1\sigma'}\Big\} \tag{255}$$

Using the properties of the projection operators, we now have

$$H_{eff} = -\frac{t^2}{U}\sum_{\sigma,\sigma'}\Big\{\hat{P}_{2\sigma}c^\dagger_{2\sigma}c_{1\sigma}\hat{P}_{1d}c^\dagger_{1\sigma'}c_{2\sigma'}\hat{P}_{2\sigma'} \tag{256}$$

$$+\hat{P}_{1\sigma}c^\dagger_{1\sigma}c_{2\sigma}\hat{P}_{2d}c^\dagger_{2\sigma'}c_{1\sigma'}\hat{P}_{1\sigma'}\Big\} \tag{257}$$

and by taking the expected value, we get a factor of one from each term, leading to $\langle\uparrow,\downarrow|H_{eff}|\uparrow,\downarrow\rangle = -2\frac{t^2}{U}$. There are several ways to proceed. One may write H_{eff} in terms of creation and annihilation operators and then express it using either

$$c^\dagger_\sigma c_\sigma = \frac{1}{2} + \sigma S^z \tag{258}$$

$$c^\dagger_\sigma c_{-\sigma} = S^x + i\sigma S^y \tag{259}$$

or introducing the so-called Hubbard operators,

$$X^{b\leftarrow a}_j = |b\rangle_j\langle a| \tag{260}$$

$$c^\dagger_{j\sigma} = X^{\sigma\leftarrow 0}_j + \sigma X^{d\leftarrow -\sigma}_j \tag{261}$$

$$[X^{b\leftarrow a}_i, X^{d\leftarrow c}_j] = \delta_{i,j}(\delta_{a,d}X^{b\leftarrow c}_j - \delta_{b,c}X^{d\leftarrow a}_j) \tag{262}$$

Here, we follow a first quantization approach to derive the same result explicitly. The matrix representation of H_{eff} in the $\{|\uparrow,\uparrow\rangle, |\downarrow,\downarrow\rangle, |\uparrow,\downarrow\rangle, |\downarrow,\uparrow\rangle\}$ basis is thus

$$\begin{pmatrix} -1 & 1 & 0 & 0 \\ 1 & -1 & 0 & 0 \\ 0 & 0 & 0 & 0 \\ 0 & 0 & 0 & 0 \end{pmatrix} \tag{263}$$

or simply

$$H_{eff} = 2\frac{t^2}{U}\big\{-|\uparrow,\downarrow\rangle\langle\uparrow,\downarrow| - |\downarrow,\uparrow\rangle\langle\downarrow,\uparrow| + |\uparrow,\downarrow\rangle\langle\downarrow,\uparrow| + |\downarrow,\uparrow\rangle\langle\uparrow,\downarrow|\big\} \tag{264}$$

or

$$\begin{aligned} H_{eff} &= 2\frac{t^2}{U}\big\{-|\uparrow\rangle_1\otimes|\downarrow\rangle_2\langle\uparrow|_1\otimes\langle\downarrow|_2 - |\downarrow\rangle_1\otimes|\uparrow\rangle_2\langle\downarrow|_1\otimes\langle\uparrow|_2 + |\uparrow\rangle_1\otimes|\downarrow\rangle_2\langle\downarrow|_1\otimes\langle\uparrow|_2 + |\downarrow\rangle_1\otimes|\uparrow\rangle_2\langle\uparrow|_1\otimes\langle\downarrow|_2\big\} \\ &= 2\frac{t^2}{U}\big\{-|\uparrow\rangle_1\langle\uparrow|\otimes|\downarrow\rangle_2\langle\downarrow| - |\downarrow\rangle_1\langle\downarrow|\otimes|\uparrow\rangle_2\langle\uparrow| + |\uparrow\rangle_1\langle\downarrow|\otimes|\downarrow\rangle_2\langle\uparrow| + |\downarrow\rangle_1\langle\uparrow|\otimes|\uparrow\rangle_2\langle\downarrow|\big\} \end{aligned} \tag{265}$$

Recall that

$$S^+_j = |\uparrow\rangle_j\langle\downarrow| \tag{266}$$

$$S^-_j = |\downarrow\rangle_j\langle\uparrow| \tag{267}$$

$$S^z_j = \frac{1}{2}\big\{|\uparrow\rangle_j\langle\uparrow| - |\downarrow\rangle_j\langle\downarrow|\big\} \tag{268}$$

then we have

$$H_{eff} = 2\frac{t^2}{U}\{-A + (S_1^+ S_2^- + S_1^- S_2^+)\} \tag{269}$$

Noting also that

$$S_1^z S_2^z = \frac{1}{4}\{|\uparrow\rangle_1 \langle\uparrow| \otimes |\uparrow\rangle_2 \langle\uparrow| + |\downarrow\rangle_1 \langle\downarrow| \otimes |\downarrow\rangle_2 \langle\downarrow| - |\uparrow\rangle_1 \langle\uparrow| \otimes |\downarrow\rangle_2 \langle\downarrow| - |\downarrow\rangle_1 \langle\downarrow| \otimes |\uparrow\rangle_2 \langle\uparrow|\} \tag{270}$$

$$\mathbb{I} = |\uparrow\rangle_1 \langle\uparrow| \otimes |\uparrow\rangle_2 \langle\uparrow| + |\downarrow\rangle_1 \langle\downarrow| \otimes |\downarrow\rangle_2 \langle\downarrow| + |\uparrow\rangle_1 \langle\uparrow| \otimes |\downarrow\rangle_2 \langle\downarrow| + |\downarrow\rangle_1 \langle\downarrow| \otimes |\uparrow\rangle_2 \langle\uparrow| \tag{271}$$

$$\mathbb{I} = |\uparrow\rangle_1 \langle\uparrow| \otimes |\uparrow\rangle_2 \langle\uparrow| + |\downarrow\rangle_1 \langle\downarrow| \otimes |\downarrow\rangle_2 \langle\downarrow| + A \tag{272}$$

Thus

$$S_1^z S_2^z = \frac{1}{4}\{\mathbb{I} - 2A\} \tag{273}$$

$$A = \frac{1}{2}(\mathbb{I} - 4S_1^z S_2^z) \tag{274}$$

$$H_{eff} = 2\frac{t^2}{U}\Big\{-\frac{1}{2}(\mathbb{I} - 4S_1^z S_2^z) + (S_1^+ S_2^- + S_1^- S_2^+)\Big\} \tag{275}$$

$$= 2\frac{t^2}{U}\Big\{-\frac{1}{2}(\mathbb{I} - 4S_1^z S_2^z) + 2(S_1^x S_2^x + S_1^y S_2^y)\Big\} \tag{276}$$

$$= 2\frac{t^2}{U}\Big\{-\frac{\mathbb{I}}{2} + 2(S_1^z S_2^z + S_1^x S_2^x + S_1^y S_2^y)\Big\} \tag{277}$$

$$H_{eff} = 4\frac{t^2}{U}\Big\{\mathbf{S}_1.\mathbf{S}_2 - \frac{\mathbb{I}}{4}\Big\} \tag{278}$$

leading to the Heisenberg Hamiltonian, which favors an AFM order.